Volume 20 | Number 16 | 28 April 2018 | Pages 10535–11486

PCCP

Physical Chemistry Chemical Physics

rsc.li/pccp

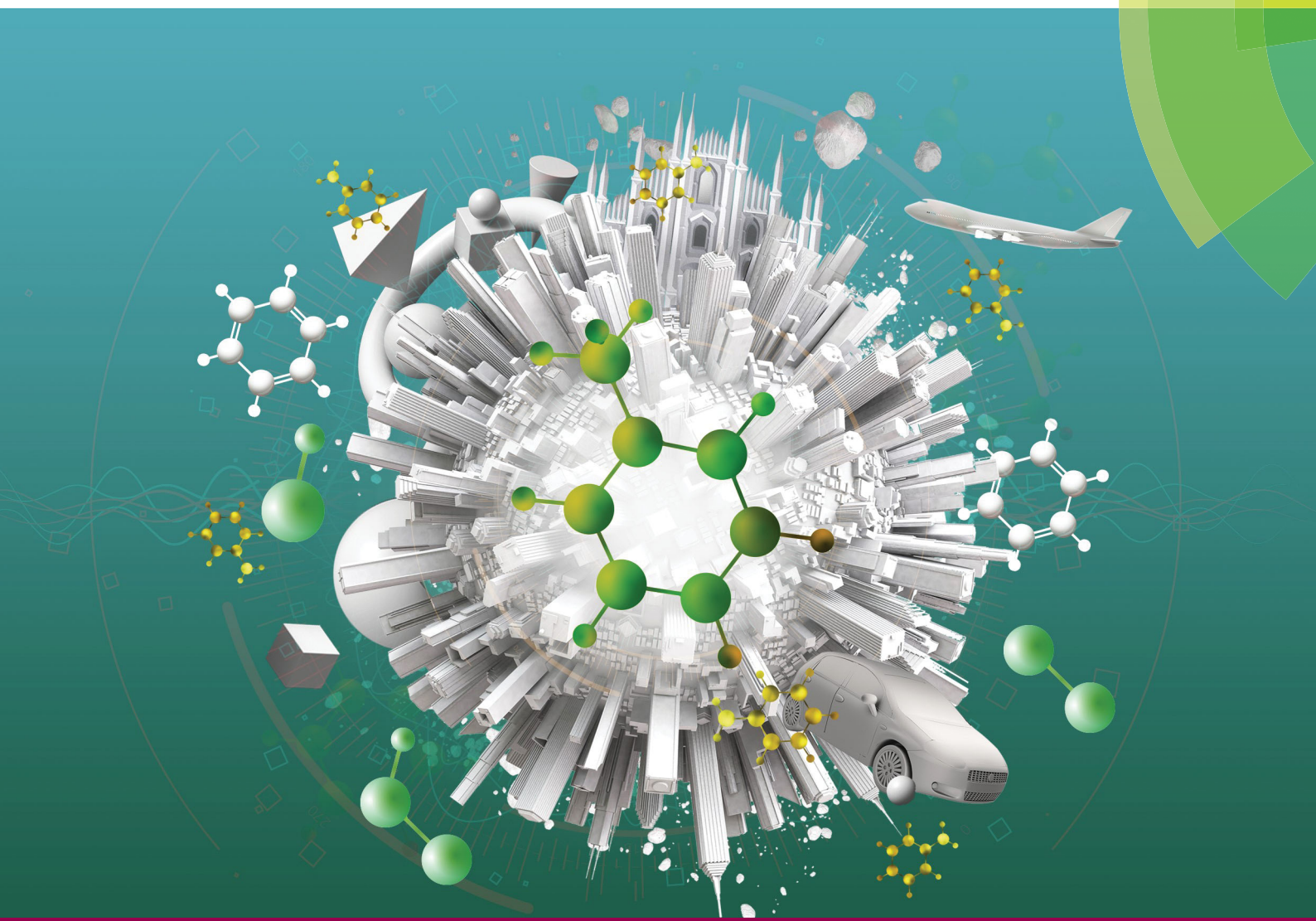

Themed issue: Bunsentagung 2018 - Kinetics in the Real World

ISSN 1463-9076

ROYAL SOCIETY OF CHEMISTRY

PAPER

M. Pelucchi *et al.*

H-Abstraction reactions by OH, HO_2, O, O_2 and benzyl radical addition to O_2 and their implications for kinetic modelling of toluene oxidation

PCCP

PAPER

View Article Online
View Journal | View Issue

Cite this: *Phys. Chem. Chem. Phys.*, 2018, **20**, 10607

H-Abstraction reactions by OH, HO_2, O, O_2 and benzyl radical addition to O_2 and their implications for kinetic modelling of toluene oxidation†

M. Pelucchi, *[a] C. Cavallotti, [a] T. Faravelli [a] and S. J. Klippenstein [b]

Received 17th November 2017,
Accepted 25th January 2018

DOI: 10.1039/c7cp07779c

rsc.li/pccp

Alkylated aromatics constitute a significant fraction of the components commonly found in commercial fuels. Toluene is typically considered as a reference fuel. Together with *n*-heptane and iso-octane, it allows for realistic emulations of the behavior of real fuels by the means of surrogate mixture formulations. Moreover, it is a key precursor for the formation of poly-aromatic hydrocarbons, which are of relevance to understanding soot growth and oxidation mechanisms. In this study the POLIMI kinetic model is first updated based on the literature and on recent kinetic modelling studies of toluene pyrolysis and oxidation. Then, important reaction pathways are investigated by means of high-level theoretical methods, thereby advancing the present knowledge on toluene oxidation. H-Abstraction reactions by OH, HO_2, O and O_2, and the reactivity on the multi well benzyl-oxygen ($C_6H_5CH_2$ + O_2) potential energy surface (PES) were investigated using electronic structure calculations, transition state theory in its conventional, variational, and variable reaction coordinate forms (VRC-TST), and master equation calculations. Exploration of the effect on POLIMI model performance of literature rate constants and of the present calculations provides valuable guidelines for implementation of the new rate parameters in existing toluene kinetic models.

1. Introduction

Alkylated aromatics such as toluene represent a significant fraction of the components in commercial gasoline, diesel and kerosene fuels. Furthermore, aromatic hydrocarbons precede the formation of poly-aromatic hydrocarbons (PAHs), which are key precursors in soot and particulate matter formation. Together with their harmful potential, the remarkable anti-knock properties (*i.e.*, high octane number, RON = research octane number, MON = motor octane number) of aromatics motivate the academic and industrial interest in better assessing their combustion properties at a fundamental level.

Historically, fuel and engine design have relied strongly on the definition of surrogate mixtures, which consist of representative components of families of species found in commercial fuels. In the case of gasoline, the surrogate fuels were commonly formulated by blending iso-octane (RON = MON = 100) and *n*-heptane (RON = MON = 0) to match the ignition propensity of a given gasoline, as characterized by its RON (*e.g.* 88–98) and MON (*e.g.* 80–88). However, as reported by Kalghatgi[1] the auto-ignition quality of a fuel is better represented by a combination of the above measures: the octane index, defined as OI = RON − *KS*. While *K* is an empirical parameter depending on the conditions of temperature and pressure, *S* represents the octane sensitivity, defined as *S* = RON − MON. Binary mixtures of PRFs are not able to fully replicate the autoignition properties of commercial octane sensitive ($S > 0$) gasolines. Therefore, toluene (RON = 120, MON = 109, $S = 11$) is typically included to represent their non-paraffinic content.

From a more fundamental kinetic modelling perspective, the development of an accurate kinetic model for toluene pyrolysis and combustion, systematically based on reaction classes and rate rules, is also of outstanding relevance for the extension to larger aromatic components in diesel (*e.g.* xylenes, methyl-naphthalene) or jet fuels (C9 alkyl aromatics), or even beyond to assess the reactivity of mono-aromatic hydrocarbons (MAH) and PAH released from biomass thermal processes.

1.1 State of the art kinetic models on toluene oxidation and kinetic analysis

The current interest of the combustion kinetics community in toluene pyrolysis and oxidation is well represented by the

[a] *Department of Chemistry, Materials and Chemical Engineering "G. Natta", Politecnico di Milano, Milan, Italy. E-mail: matteo.pelucchi@polimi.it*
[b] *Chemical Sciences and Engineering Division, Argonne National Laboratory, Argonne, IL, USA*

† Electronic supplementary information (ESI) available. See DOI: 10.1039/c7cp07779c

recent studies of Yuan *et al.*[2,3] and of Zhang *et al.*[4] In a first study, Yuan and co-workers presented new experimental measurements of both toluene pyrolysis and oxidation.[2] Pyrolysis was studied in a flow reactor at pressures up to atmospheric and temperatures in the range 1100–1730 K. Intermediate and product species were analyzed using synchrotron vacuum ultraviolet photoionization mass spectrometry. The oxidation was investigated in a jet stirred reactor (JSR) at 10 atm pressure and temperatures from 950 to 1200 K using gas chromatography combined with a flame ionization detector, a thermal conductivity detector and mass spectrometry. Based on the literature, a detailed kinetic model of toluene combustion was developed to reproduce the decomposition of toluene and growth of aromatics in both the flow reactor pyrolysis and JSR oxidation. A subsequent study from the same group[3] presented a complete validation of the detailed kinetic model by comparison with a large number of validation targets available in the literature.[2–19]

More recently, Zhang *et al.*[4] presented an experimental and kinetic modelling study of toluene/dimethyl ether mixtures over a broad range of conditions (T = 630–1460 K, p = 20 and 40 atm) in shock tubes and rapid compression machines. Dimethyl ether was chosen as the low-octane component to blend with toluene because of its favorable vapor pressure and its relatively simple kinetic model (*i.e.*, low number of thermochemical parameters). Recent studies on toluene oxidations, comprising this work, stemmed primarily from the consideration that different toluene kinetic models available in the literature showed quite controversial behaviors in terms of ignition propensity. Fig. 1, adapted and extended from the studies of Somers *et al.*[20] and of Zhang *et al.*,[4] effectively summarizes such observations. At low temperatures (T < 1000 K) existing toluene models span orders of magnitude in terms of ignition delay time predictions. More recent models[2–4,21] converge at T > 1000 K, while still differing by orders of magnitude at lower temperatures.

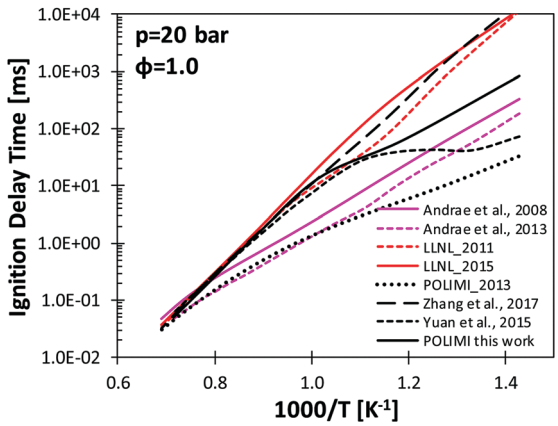

Fig. 1 Predictions of Ignition delay times for φ = 1.0 toluene/air mixtures at p = 20 atm using different models available in the literature,[4,21–24] and the updated POLIMI model from this study.

As highlighted in the axonometric view of Fig. 2, which schematically shows the conditions of temperature, pressure and equivalence ratio experimentally investigated in the literature,[2–19] there is still no experimental data for pure toluene at temperatures below ~980 K. This limitation largely arises from the complexity of studying toluene experimentally, both because of its low vapor pressure (~0.038 atm at T = 298 K) and its strong resistance to autoignition (*i.e.*, high octane number) briefly discussed above. The lack of validation targets for pure toluene at lower temperatures leads to substantial differences in the models as seen in Fig. 1, and motivates the present theoretical effort to estimate the key reaction rate constants as a means to better understand toluene combustion kinetics.

Sensitivity plots of ignition delay times for a toluene/air stoichiometric mixture at p = 20 bar and three different temperatures (T = 689, 1044 and 1400 K) (*cf.* Fig. 3) further confirm the large variability of the dominant reactions within recently developed mechanisms.[2–4] To obtain a very general but still significant overview, the sensitivity coefficients, obtained as discussed in Cuoci *et al.*,[25] have been normalized to the most sensitive reaction at each temperature. Thereof, the ten most sensitive reactions have been selected by averaging, over the three investigated temperatures, the absolute values of the normalized sensitivity coefficients. A positive sensitivity coefficient

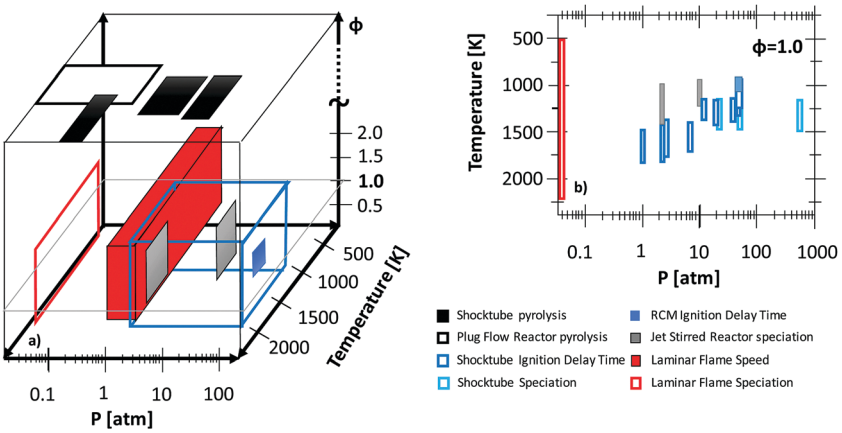

Fig. 2 Axonometric and bi-dimensional (φ = 1.0) views of the experimental measurements available in the literature for toluene oxidation and pyrolysis.[2–19]

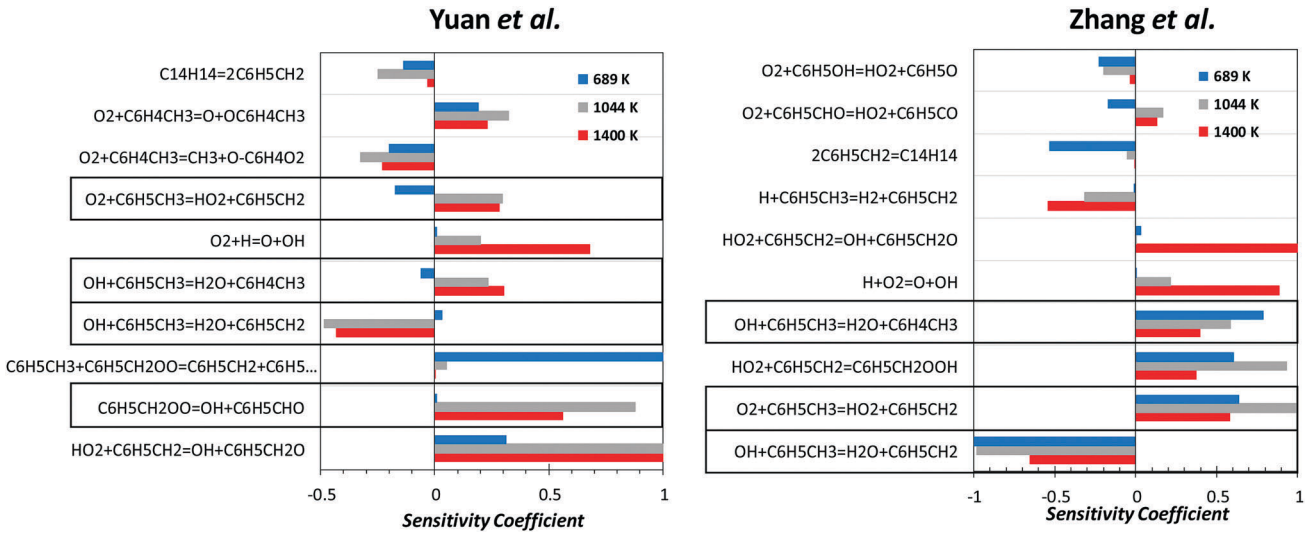

Fig. 3 Normalized sensitivity coefficients of temperature increase to rate constants in the mechanisms from Yuan *et al.*[2,3] and Zhang *et al.*[4] Black boxes highlight key reaction pathways investigated in this study. Batch reactor constant volume simulations.

correlates with a reaction that increases reactivity (*i.e.*, lowers the ignition delay time) and *vice versa*.

Prior to any theoretical calculations, the toluene subset of the Politecnico di Milano (POLIMI) mechanism[22,26] was updated based on theoretical and/or experimental determinations of rate constants presented in the literature.[27–44] Fig. 4 reports results from sensitivity analysis carried out with the POLIMI starting mechanism at the same conditions of Fig. 3.

Despite many differences emerging from this first analysis, some common features are highlighted. First, the relative branching between H-abstraction by OH forming benzyl radical ($C_6H_5CH_2$) and that forming the lumped methyl-phenyl radical ($C_6H_4CH_3$) plays a critical role in determining toluene ignition propensity. H-Abstraction by $^3O_2$ to form HO_2 and benzyl radical enhances ignition at intermediate (T = 1044 K) and high temperature (T = 1400 K). At lower temperatures, instead, a more or less pronounced inhibiting effect is observed. In fact, due to its endothermic nature, this reaction pathway proceeds in the forward direction (producing two radical species from two stable molecules) at high temperatures (~above 1000 K), while it is shifted backward at lower temperatures, where it acts as a termination step. As recently discussed by Zhou *et al.*,[45] this particular reaction class plays a very important role in the oxidation of fuel molecules having allylic hydrogen atoms (*i.e.*, propene, iso-butene *etc.*), or benzylic hydrogen atoms as is the case for toluene. Other important H-abstraction reactions are those by $O(^3P)$ and HO_2, which are important not only for toluene or reference fuel mixtures oxidation, but, more generally for MAH and PAH species oxidation, where strong interactions with the aromatic ring may exist.

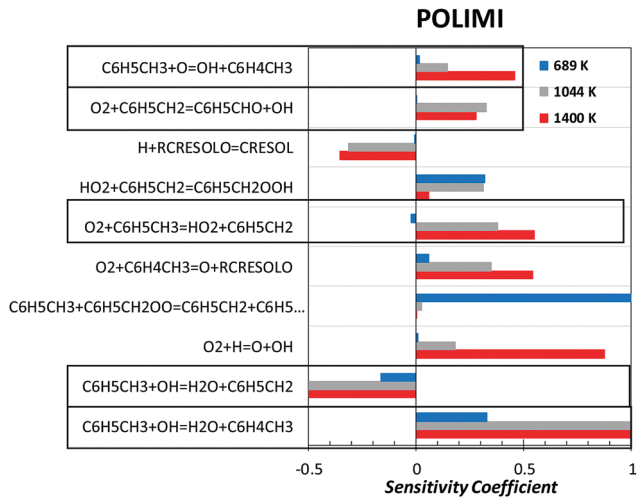

Fig. 4 Normalized sensitivity coefficients of temperature increase to rate constants in the POLIMI starting mechanism. Black boxes highlight key reaction pathways investigated in this study.

According to the standard low temperature oxidation pathways in aliphatic hydrocarbons (*n*-, iso- and cyclo-alkanes),[46,47] once a fuel molecule undergoes an H-abstraction, the fuel radical can interact with O_2, forming peroxy radical species. The competition between successive isomerization, decompositions and second oxygen addition govern the transition between phenomena such as low temperature branching (cool flames), negative temperature coefficient and high temperature pathways; greatly impacting the operability and efficiency of real combustion devices.[1] Thus, for toluene, the interactions of benzyl and methyl-phenyl radical with O_2 are important. Due to the stability of benzyl radical compared to other radicals (*e.g.* alkyl radicals), its reaction pathways and kinetics are somewhat atypical. Thus, the combination of its barrierless addition to O_2, the stabilization of the peroxy radical (benzyl-peroxy radical, $C_6H_5CH_2OO$), the backward decomposition to reactants and other possible decomposition channels constitute additional important features to be assessed in toluene kinetic models.

Theoretical kinetics calculations for the $C_7H_7 + O_2$ systems were presented around the same time by da Silva *et al.*[41] and by Murakami *et al.*,[38] focusing on $C_6H_4CH_3 + O_2$ and on $C_6H_5CH_2 + O_2$, respectively. Da Silva *et al.*[41] suggested that the dominant reaction products in the chemically activated methylphenyl + O_2 systems are methylphenoxy and O radicals ($O_2 + C_6H_4CH_3 = O + OC_6H_4CH_3$) and methyl-dioxo-hexadienyl radicals from ring opening. Murakami *et al.*[38] found that the dominant decomposition channel of benzyl peroxy radical was $C_6H_5CH_2OO = C_6H_5CHO + OH$; appearing as one of the most sensitive reactions in Fig. 3 for the mechanism of Yuan *et al.*[2,3] The rate constants from these previous studies are adopted in the state-of-the-art models by Yuan *et al.*[2,3] and Zhang *et al.*[4] More recently, Zhang *et al.*[48] systematically analyzed the O_2 recombination kinetics for a number of representative aromatic radicals including benzyl radical. These calculations should provide a highly accurate baseline for the $C_6H_5CH_2 + O_2$ reaction.

Following the theoretical studies of da Silva and co-workers, recent kinetic models find some consensus on the predominant reaction pathways of benzyl radical. According to the theoretical calculations, $C_6H_5CH_2$ is largely oxidized by recombination with HO_2, leading to the formation of benzylhydroperoxide ($C_6H_5CH_2OOH$) at temperatures lower than $\sim$750 K, or benzoxyl radical and OH for higher temperatures. These rate constants were updated by Zhang *et al.*[4] who determined pressure-dependencies for each pathway using QRRK theory with a modified strong collision approximation accounting for collisional energy transfer.[49] While these pathways result in an increased reactivity, self-recombination of benzyl radicals to form bibenzyl ($C_{14}H_{14}$) or recombination with methyl radical producing ethylbenzene clearly reduce reactivity by terminating the radical propagation.

The overall POLIMI mechanism (484 species and 13190 reactions) implements a C0–C3 core mechanism obtained by coupling the H_2/O_2 subset from Keromnes *et al.*,[50] C_1/C_2 from Metcalfe *et al.*,[51] and C_3 from Burke *et al.*,[52,53] and Ranzi *et al.*[22,26] The thermochemical properties were adopted, when available, from the ATcT database of Rusic *et al.*[54,55] or from Burcat's database.[56] The kinetic mechanism with thermodynamic and transport properties is reported in the ESI,† together with an extensive comparison with experimental targets.

1.2 Goals of this study

This study aims to:

(1) Provide new accurate rate constants for H-abstraction reactions by $O(^3P)$, OH, HO_2 and $^3O_2$ from high level theoretical calculations.

(2) Reinvestigate the potential energy surface of the $C_6H_5CH_2 + {}^3O_2$ system with higher level theoretical methods and obtaining temperature and pressure dependent rate constants.

(3) Assess the impact of these new rate parameters on model predictions by modeling a few selected validation targets.

(4) Present and validate the POLIMI kinetic model for toluene pyrolysis and oxidation.

(5) Highlight needs and future challenges for the kinetic modeling of toluene.

2. Method

H-Abstraction reactions and the reactivity on the benzyl-oxygen multiwell potential energy surface (PES) were investigated using electronic structure calculations, transition state theory in its conventional, variational, and variable reaction coordinate forms (VRC-TST), and master equation calculations.

For the H-abstraction reactions, the geometries and frequencies for all stationary points, including van der Waals wells, were determined with density functional theory (DFT) using the M06-2X functional[57] and the 6-311+G(d,p) basis set. Energies were calculated at the M06-2X geometries with the CCSD(T) method[58] using the aug-cc-pVTZ basis set.[59] This CCSD(T) energy was corrected for basis set effects by adding the difference between energies computed at the density fitting (DF) MP2 level using the aug-cc-pVQZ and aug-cc-pVTZ basis sets:[60]

$$E = E_{\text{CCSD(T)/aug-cc-pVTZ}} + E_{\text{DF-MP2/aug-cc-pVQZ}} - E_{\text{DF-MP2/aug-cc-pVTZ}}.$$

Special care was placed in describing internal rotations. Energies for torsional motions were obtained from relaxed scans at 20° intervals performed at the M06-2X/6-311+G(d,p) level. The corresponding partition functions were then determined using one-dimensional or, when appropriate, two dimensional hindered rotor models, as implemented in the PAPR suite of codes.[61] In particular, 2-dimensional hindered rotors were considered for H-abstractions from methyl by OH and $^3O_2$.

For all reactions considered here, intrinsic reaction coordinate (IRC) calculations were performed with a step size of $\sim$0.016 Å, taking 30 steps toward the products and 30 toward the reactants. For each point Hessians were computed and frequencies determined after projecting out torsional motions, as suggested by Green and co-workers.[62] IRC calculations were used to confirm that the saddle points connect the desired reactants and products and, more importantly, to determine a variational correction to the rate constants. Tunneling corrections were computed using the asymmetric Eckart model.

The transition state for essentially any abstraction is preceded and followed by van der Waals wells, with corresponding transition states for the formation and decay of these complexes. These van der Waals wells have various effects on the kinetics including the introduction of some pressure dependence, albeit only at rather high pressures, and, perhaps more importantly, in modulating the details of tunneling. Master equation treatments that include these wells, as implemented here, provide a proper treatment of their effect on the kinetics. These effects include a limitation of the convolution over energy to energies that exceed the asymptotic energies of the reactants and products (at least at low pressure) and more generally a constraint on the reactive flux to less than that for the van der Waals complex formation. Here, the formation of van der Waals wells for the entrance channel was considered for all H-abstractions from the methyl group, as these reactions are significantly faster than abstraction

from the ring at low temperatures. In this case, tunneling effects are expected to be relevant and an accurate estimation of the forward and reverse barrier heights is then necessary. The present analysis is thus not exhaustive for what concerns the identification of all the van der Waals wells that can be formed between toluene and the abstracting reactants, as only those that can have a significant impact on the rate constant calculations in the investigated temperature and pressure ranges were included in the calculations. In the case of HO_2 abstraction from the methyl group, the van der Waals well on the product side was also included in the calculations. The rates of formation and decomposition of van der Waals wells were determined using phase space theory, as implemented in the Mess code.[61]

For oxygen addition to benzyl, geometries, frequencies, and zero point energies for reactants, wells, products, and transition states were determined at the B2PLYP-D3[63] level of theory using the cc-pVTZ basis set. Energies were determined for the B2PLYP-D3 geometries at the CCSD(T)-F12/VTZ-F12 level[64,65] and a correction for basis set effects was obtained from the difference between MP2-F12/VQZ-F12[66] and MP2-F12/VTZ-F12 energies: $E = E_{\text{CCSD(T)-F12/VTZ-F12}} + E_{\text{MP2-F12/VQZ-F12}} - E_{\text{MP2-F12/VTZ-F12}}$. For the barrierless entrance channel ($C_6H_5CH_2 + O_2 = C_6H_5CH_2OO$), we used the VRC-TST transition state partition functions recently determined by Zhang *et al.*[48,67] Rate coefficients were calculated for the 300–2500 K range of temperatures and for the 0.1–1000 bar range of pressure by solving the 1D master equation. The collisional energy transfer probability was described with the exponential down model, with $\Delta E_{\text{down}} = 260\ (T/300)^{0.875}$ (cm^{-1}) assuming an argon bath gas, which is consistent with literature values for the room temperature energy transfer parameters for toluene[68] and the temperature dependence for reactions of hydrocarbons with oxygen or HO_2.[69] Quantum tunneling contributions to the rate constant were again estimated from the Eckart model.

All DFT calculations were performed using Gaussian G09,[70] all MP2, CCSD(T), and CASPT2 calculations were performed using Molpro 2015,[71] and all master equation calculations were done using the MESS solver.[61] ME input files were generated using a new code, EStokTP, designed to perform automatically the investigation of the torsional conformation space, to project torsional motions from Hessians, and determine 1-D and multidimensional PES for rotors.[72] The input files for all master equation and transition state theory calculations are reported as ESI† to this paper.

The calculated rate coefficients were fitted to the modified Arrhenius expression as:

$$k = AT^n \exp\left(\frac{-E_a}{RT}\right)$$

The impact of the calculated rate constants on our reference kinetic mechanism is finally analysed through detailed kinetic simulations. In these simulations, several rates constants, grouped as a function of the abstracting radical or individually as $^3O_2$ addition to benzyl, are varied and the impact on the ignition delay times and toluene concentration profiles are examined under a variety of conditions. The intent is to evaluate how much the modification of a rate constant with respect to literature values can affect the performance of a complex mechanism and in which direction. Kinetic simulations were performed using the OpenSMOKE++ suite of programs.[25]

3. Results and discussion

This section describes the theoretical investigation of H-abstraction reactions by OH, HO_2, $O(^3P)$ and $^3O_2$ (Section 3.1) and of the reactions on the $C_6H_5CH_2 + {}^3O_2$ potential energy surface (Section 3.2); providing rate constants for direct use in toluene kinetic models. The presentation of the results for H-abstraction reactions is preceded by a section reporting the 0 K energies of the C–H bonds in toluene.

3.1 H-Abstraction reactions by OH, HO_2, $O(^3P)$ and $^3O_2$

3.1.1 C–H bond dissociation energies in toluene. The C–H bond dissociation energies (BDE) in toluene were predicted from calculations of $E = E_{\text{CCSD(T)-F12/VTZ-F12}} + E_{\text{MP2-F12/VQZ-F12}} - E_{\text{MP2-F12/VTZ-F12}}$ for geometries determined at the M06-2X/6-311+G(d,p) level of theory. The computed 0 K bond energies are reported in Fig. S1 (ESI†) together with nomenclature and optimized structures for the derived radicals. The C–H BDE for the methyl group of toluene has been the subject of both experimental and theoretical investigations in the literature. The value computed here, 88.6 kcal mol^{-1}, is in good agreement with the experimental value of Ellison *et al.* of 88.1 ± 0.5 kcal mol^{-1},[73] thus suggesting that the level of theory chosen to study this system is appropriate, at least in terms of description of the bond energetics. Notably, the C–H bond in the methyl group is ~22 kcal mol^{-1} weaker than those located on the ring. H-Abstraction from this site produces the resonance-stabilized benzyl radical ($C_6H_5CH_2$), which partly explains the negative sensitive coefficients highlighted in Fig. 3 and 4. The three ring positions (*ortho*-, *meta*-, *para*-) have very similar BDEs, with the formation of *para*-methylphenyl radical being slightly unfavored (~0.5 kcal mol^{-1}). This suggests that abstraction from the methyl group may be expected to be favored over abstraction from the ring. As will be shown in the following, while this is the case at low temperatures, H-abstraction from the ring acquires relevance as the temperature increases because of significant enthalpy–entropy compensation effects.

3.1.2 H-Abstractions by OH. Several experimental investigations have been reported for the OH + $C_6H_5CH_3$ reaction both at very low temperatures ($T < 400$ K)[74,75] and at higher temperatures (400 K < T < 1500 K).[27,76–78] Seta *et al.*[27] investigated the rate constants for H-abstractions, addition and H/OH substitution reactions by means of an effective coupling of TST and experiments. Single point energies were calculated at the G3(MP2)//B3LYP and CBS-QB3 levels. The heights of the TS barriers were adjusted to reproduce the high temperature measurements, providing a reliable set of rate constants that have been adopted to a great extent in the more recent toluene kinetic mechanisms.[2–4] A very recent study by Li *et al.*[44]

Table 1 Relative energies of transition states and products. Units are kcal mol^{-1}

Transition state	This work	Li *et al.*	Seta *et al.*	Products	This work	Li *et al.*	Seta *et al.*
TS_{METHYL}	0.6	1.2	0.6[a]	$C_6H_5CH_2 + H_2O$	−28.3	−28.5	−29.3
TS_{ortho}	3.5	3.2	2.4	o-$C_6H_4CH_3 + H_2O$	−6.1	−6.2	−6.3
TS_{meta}	3.8	3.5	3.1	m-$C_6H_4CH_3 + H_2O$	−6.2	−6.1	−6.4
TS_{para}	4.0	3.6	2.7	p-$C_6H_4CH_3 + H_2O$	−5.7	−5.6	−5.2

[a] The energy barrier from Seta *et al.*[27] for the benzyl formation channel here reported is derived by best fit to experimental rate constants.

provided rate constants for H-abstraction reactions by OH, H, $O(^3P)$, HO_2 and CH_3 using energies and structures determined using the G4 hybrid method.

The potential energy surface (PES) for H-abstraction reactions by OH is reported in the ESI† (Fig. S2). In contrast with Seta *et al.*,[27] who considered the formation of van der Waals complexes only when the barrier was submerged, and the recent study of Li *et al.*,[44] we were able to identify an entrance van der Waals well for abstraction from methyl that is about 3 kcal mol^{-1} more stable than the reactants. In the case of abstraction from the methyl group, the transition state lies 0.6 kcal mol^{-1} above the reactants and thus 3.6 kcal mol^{-1} above the entrance well. H-Abstractions from the different ring positions have comparable barriers (3.5–4.0 kcal mol^{-1}) with respect to the reactants, but a much lower exothermicity compared to H-abstraction from the methyl group.

Table 1 compares the relative energy barrier and energy changes with those calculated in previous studies.[27,44] It is to be noted that in the work of Seta *et al.*[27] the barrier for H-abstraction from the CH_3 group was adjusted, to provide better agreement with the measurements. Good agreement is found between the three studies (±1.3 kcal mol^{-1}).

Fig. 5a compares the total H-abstraction rate constant from this study with measurements and other theoretical studies from the literature. At low temperatures, experimental measurements of the OH + toluene reaction rate[74,75,78] generally observe a significant contribution from the addition channel. For the purposes of comparison, any experimental data points that are likely affected by such addition channels were not included in the plot of Fig. 5a. Perry *et al.*[75] reported that the addition channel becomes ineffective above 380 K. According to Tully *et al.*[77] H-Abstraction is the dominant reaction for $T > 450$ K. Markert *et al.*[74] measured a total rate constant for OH + toluene of $(3.85 \pm 0.42) \times 10^{12}$ cm^3 mol^{-1} s^{-1} at $T = 338$ K. From the relative concentrations of benzyl radical and of the adduct they defined a relative branching for H-abstraction/addition of 0.11/0.89 at $T = 338$ K. Also Knispel and co-workers[78] measured specific contributions from the two competing channels.

The calculations are in very good agreement with the experimental data; providing a smooth reproduction of the somewhat disparate experimental values and with maximum discrepancies of a factor of 2. Moreover, the agreement with the rate constant of Seta *et al.*[27] is within a factor of ~1.35. Again, it should be noted that Seta *et al.* obtained good agreement through an energy barrier adjustment. G3(MP2)//B3LYP provided a barrier of ~2.77 kcal mol^{-1}, a lower barrier (~1.33 kcal mol^{-1}) was obtained with CBS-QB3 calculations and the final value of ~0.6 kcal mol^{-1} was obtained by best fit to the experimental measurements. The accuracy of our *a priori* determination provides some validation of our theoretical predictions for other abstracting radicals and for the branching in this reaction, all of which are based on the same methodology. The rate constants from Seta *et al.*[27] were adopted and modified by Zhang *et al.* to improve the agreement with ignition delay time measurements.

Fig. 5b shows the branching ratio between H-abstraction from the ring leading to the formation of methylphenyl radicals ($C_6H_4CH_3$) and benzyl radical ($C_6H_5CH_2$). Benzyl radical formation

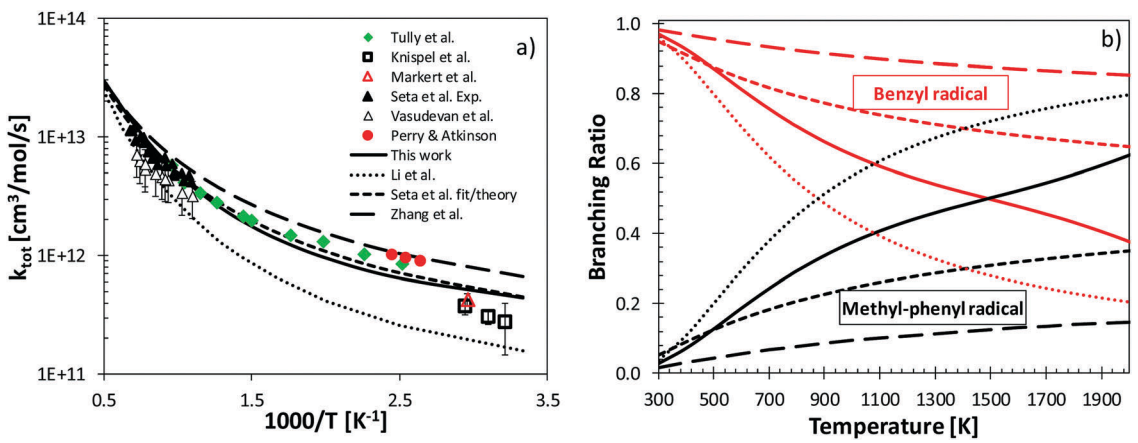

Fig. 5 Left panel: Comparison of the total rate constant for H-abstraction by OH with other studies[4,27,44] and with experimental measurements.[27,74–78] Right panel: Branching ratio between benzyl radical ($C_6H_5CH_2$) and methylphenyl radicals ($C_6H_4CH_3$).

dominates up to ~1500 K where a crossover is observed. This is intermediate between that proposed by Li *et al.*,[44] who predicted a crossing at about 900 K, and Seta *et al.*[27] who found that the formation of benzyl is always dominant. The difference between the previous and present rate constant predictions may be due, in the case of Seta *et al.*, to our use of a more detailed model for internal rotations; in particular for the OH torsional motion at the saddle point. Regarding the estimates of Li *et al.*,[44] the difference is most likely related to the barrier heights, since our predicted barriers are slightly larger for abstraction from the ring (by 0.3 kcal mol^{-1}) and smaller for abstraction from methyl (by 0.6 kcal mol^{-1}), with a net difference for the branching of about 0.9 kcal mol^{-1}. The better agreement we observe with experimental data at low temperatures (Fig. 5), where the rate constant is most sensitive to the height of the energy barrier, suggests that the 0.6 kcal mol^{-1} energy barrier we computed for abstraction from methyl is probably more accurate.

Regarding the branching ratios suggested by Zhang *et al.*,[4] as clearly discussed by the authors, the rate constants of Seta were increased by a factor of ~1.6 and decreased by a factor of ~0.5 for the channels leading to benzyl radical and methyl-phenyl. These modifications were incorporated to improve the agreement with experimental data in the kinetic simulations. As will be shown below in Section 4, such revisions may be no longer necessary if the updated rate constants proposed in this work are used in the simulations.

The calculated rate constants were fitted in the temperature range 300–2500 K and are reported in Table S1 of the ESI,† together with the other H-abstraction channels computed in the present work.

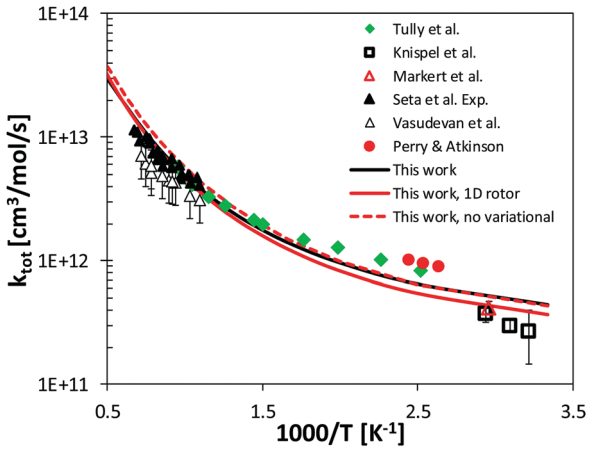

Fig. 6 Effect of using different levels of theory in the estimation of H-abstraction rate constants for OH + toluene. Experimental data (symbols) from.[27,74–78]

Fig. 6 shows the impact of using different levels of theory in the estimation of the total abstraction rate constant. It can be observed that variational effects decrease the rate constant by 5% at low temperatures and 30% at the highest, while the description of torsional motions using the 2D rotor model (labelled this work) increases the rate constant with respect to the 1D hindered rotor model by 20% at low temperatures and, although not shown in the temperature range reported in Fig. 6, decreases it by a factor of about 2 at 2500 K.

To test the impact of the level of theory used to locate van der Waals wells, structures and vibrational frequencies of the entrance well for H-abstraction from methyl were determined at the WB97-XD/6-311+G(d,p) and B2PLYP-D3/6-311+G(d,p) levels. The ZPE corrected CCSD(T) energies of the wells calculated relative to the reactants on M06-2X, B2PLYP-D3, and WB97X-D geometries were −3.03, −2.55, and −2.48 kcal mol^{-1}, respectively. It is interesting to note that M06-2X performs better in locating the minimum energy structure than two functionals that explicitly include dispersion corrections. This is in agreement with previous theoretical studies indicating that, thanks to its parameterization aimed at mimicking both short and intermediate range dispersion effects, the M06-2X functional performs relatively well in predicting structures and energies of van der Waals complexes.[79]

3.1.3 H-Abstractions by HO_2. The application of predictive theory for reactions that are challenging, or even impossible, to study experimentally was recently discussed by Klippenstein.[80] Typical examples are H-abstractions by HO_2. The potential energy surface for toluene H-abstraction reactions by HO_2 as obtained in this study is reported in Fig. S3 of the ESI.†

Table 2 compares the relative energies of the PES in Fig. S3 (ESI†) with those from Li *et al.*[44] Again, the deviations are within the uncertainty of the different theoretical methods.

Beside the recommended values of Baulch *et al.*,[81] H-abstractions by HO_2 from toluene have been investigated theoretically only by Altarawneh *et al.*[82] and very recently by Li *et al.*[44] Altarawneh *et al.* studied this system at the BB1K/6-311+G(d,p) level of theory. Consistent with the observations of Li *et al.*,[44] product-like van der Waals complexes slightly more stable than the products (~1.5 kcal mol^{-1}) exist for abstractions from the ring. However, such complexes were neglected in previous studies, instead assuming direct dissociations to methyl-phenyl radicals.

Fig. 7a compares the total H-abstraction rate constant calculated in this work with the values computed by Li *et al.*[44] and those adopted in the mechanisms of Yuan *et al.*[2,3] and

Table 2 Relative energies of transition states and products for HO_2 + toluene H-abstraction reactions. Units are kcal mol^{-1}

Transition State	This work	Li *et al.*	Products	This work	Li *et al.*
TS_{METHYL}	14.2	13.5	$C_6H_5CH_2 + H_2O_2$	2.8	2.8
TS_{ortho}	23.6	22.7	o-$C_6H_4CH_3 + H_2O_2$	25.0	25.1
TS_{meta}	24.0	23.3	m-$C_6H_4CH_3 + H_2O_2$	25.0	25.2
TS_{para}	24.4	23.7	p-$C_6H_4CH_3 + H_2O_2$	25.5	25.7

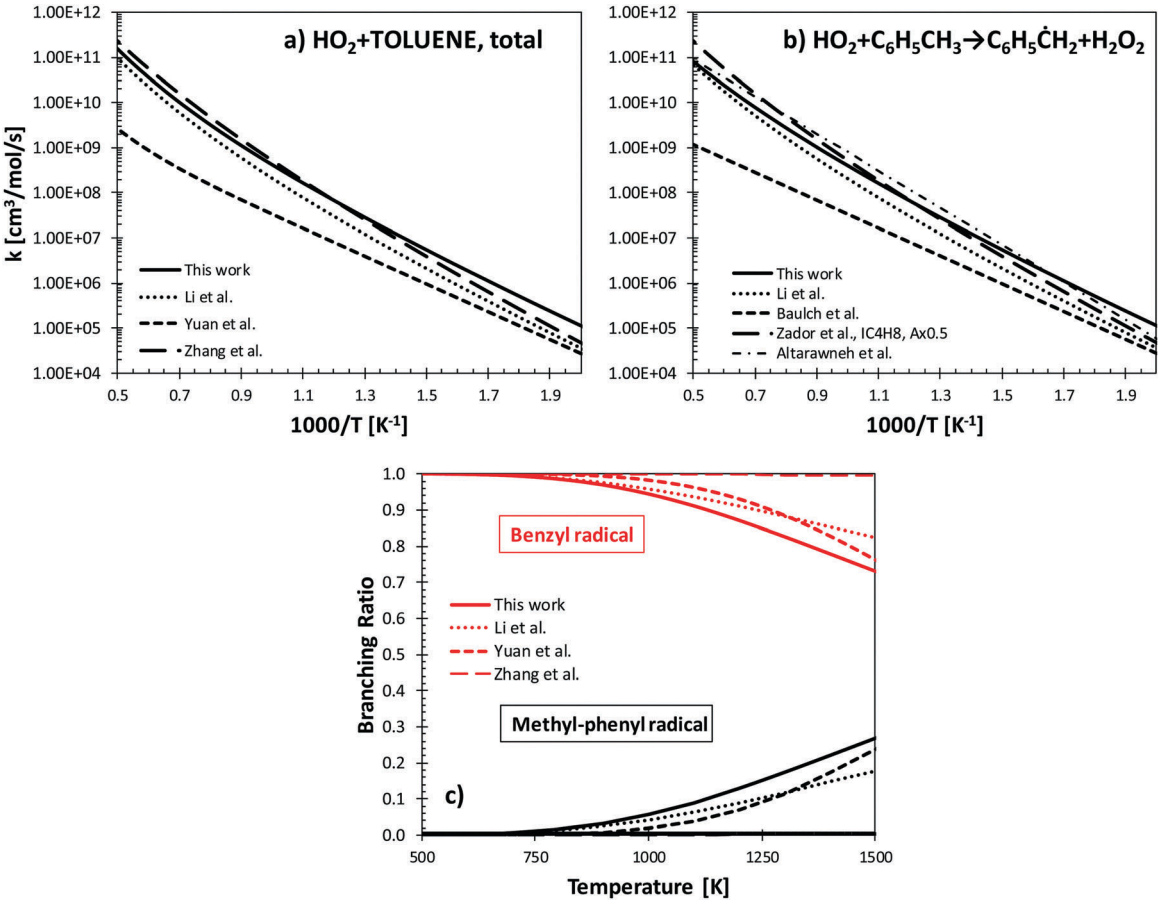

Fig. 7 Panel a: Comparison of the total abstraction rate constant for HO_2 + toluene with other theoretical studies[44] and those used in toluene kinetic models.[2–4] Panel b: Comparison of H-abstraction by HO_2 to form benzyl radical from this study with other studies.[81–83] Panel c: Branching ratios between benzyl radical (red lines) and methyl-phenyl radical lumped isomer (black lines) according to different studies.

Zhang *et al.*[4] In the case of Yuan *et al.*, the value proposed by Baulch *et al.*[81] and that from Altarawneh *et al.*[82] were decreased by a factor of 4. The value proposed by Baulch for the H-abstraction from the methyl group (Fig. 7b) is about 5–10 times lower than other estimates at 900–1100 K, explaining the large deviation in the total rate constant adopted by Yuan. Based on similarity, the Zhang *et al.* mechanism implements the rate constant of Zador *et al.*[83] for HO_2 + iso-butene, with an adjustment to the exponential factor to account for the single methyl group available in toluene. Again, the adjusted rate of Altarawneh *et al.* is adopted for the channel forming methyl-phenyl radicals. Overall, the total rate of abstraction agrees within a factor of ~2 with this work and with the work of Li *et al.*[44] In terms of relative branching, however, Zhang *et al.* strongly favor the formation of benzyl radical, accounting for 100% over the whole temperature range. In agreement with other estimates, we predict the formation of benzyl to be generally preferential, mainly in the temperature range where H-abstractions by HO_2 are of relevance (900–1100 K), but a non negligible competition exists with the formation of methyl-phenyl radicals.

3.1.4 H-Abstractions by O(^{3}P). The triplet potential energy surface for toluene H-abstraction reactions by O(^{3}P) is provided as ESI† (Fig. S4). The three lowest electronic energy levels, having a multiplicity of 5, 3, and 1, have been accounted for in the evaluation of the electronic partition function for the reactant, while both the ground and the first excited state, which are triplets, were considered for the saddle point. The energy difference between the ground and excited states was computed at the multireference CASPT2 level for state-averaged two-states CASSCF wavefunctions at M06-2X/6-311+G(d,p) geometries. Two active spaces were used in the calculations: (6e,5o), including the four electrons and three p orbitals of oxygen and the σC–H bonding and antibonding orbital of the reacting hydrogen; (12e,11o), obtained by supplementing the (6e,5o) active space with the π electrons and orbitals (bonding and antibonding) of the aromatic ring. Calculations were performed with a 0.2 energy shift using both single state single reference (SS-SR) and multi state multi reference (MS-MR) (only for the (6e,5o) active space) methods.[84] The SS-SR and MS-MR calculations for the (6e,5o) active space were in nice agreement (within 0.1 kcal mol^{-1}), so that the energy of the first excited state was computed using the largest active space and the aug-cc-pVTZ basis set. The results of the calculations are reported as ESI† in Table S2.

H-Abstraction from the methyl group has a barrier of ~5.2 kcal mol^{-1}, which is ~4.3–4.8 kcal mol^{-1} lower than that for abstraction from the ring. The excited state energy

Table 3 Relative energies of transition states and products for $O(^3P)$ + toluene H-abstraction reactions. The excited state energy barriers are reported between parentheses. Units are kcal mol^{-1}

Transition state	This work	Li *et al.*	Products	This work	Li *et al.*
TS_{METHYL}	5.2 (5.5)	4.2	$C_6H_5CH_2$ + OH	−12.4	−13.6
TS_{ortho}	9.5 (10.2)	9.6	*o*-$C_6H_4CH_3$ + OH	9.8	8.7
TS_{meta}	9.8 (10.6)	9.7	*m*-$C_6H_4CH_3$ + OH	9.8	8.8
TS_{para}	10.1 (10.9)	10.0	*p*-$C_6H_4CH_3$ + OH	10.3	9.3

barrier is 0.33 kcal mol^{-1} higher than that of the ground state for abstraction from methyl and about 0.75 kcal mol^{-1} for abstraction from the ring.

Other than this study, the only theoretical investigation in the literature is that from Li *et al.*[44] The energy barriers and 0 K energy changes are compared in Table 3. The agreement is very good except for the H-abstraction barrier from the methyl group, which is about 1 kcal mol^{-1} higher than computed by Li *et al.*[44]

H-Abstraction by $O(^3P)$ was investigated experimentally by Hoffmann *et al.*[85] in shock tubes for a narrow temperature range (1150–1300 K) at pressures of ~0.5 atm. Overall, based on OH profile measurements, the H-abstraction channels were found to account for ~10% of the total O + $C_6H_5CH_3$ reactions. The remaining 90% of toluene consumption was attributed to O addition. As in Yuan *et al.* and in Zhang *et al.*,[2–4] the O addition reactions to the aromatic ring have been adopted from the study of Taatjes *et al.*[86] within the updated POLIMI model.

Starting from the same parameters for the addition reactions,[86] Fig. 8 compares the experimental values for both the H-abstraction channels (symbols) and the total rate constant for O + $C_6H_5CH_3$ as obtained by Hoffmann *et al.*,[85] with different sets of H-abstraction reactions. Despite the improvements compared to the work of Li *et al.*,[44] the experimental results of Hoffmann *et al.*[85] are still overestimated by a factor of ~2–3. It should however be mentioned that Hoffmann *et al.* determined the H-abstraction rate by using a kinetic mechanism to fit the experimental data. One of the sensitive reactions for their mechanism was OH abstraction from toluene to give benzyl. The value adopted there is about 3–4 times larger than determined in the present study, thus suggesting that the contribution of the O + toluene H-abstraction reaction to the formation of benzyl and OH may have been significantly underestimated because of the overestimation of the rate of the competitive process.

As shown in Fig. 9, according to our calculations the formation of benzyl radical dominates for temperatures up to ~1600 K. According to Li *et al.*,[44] H-abstraction from the ring is

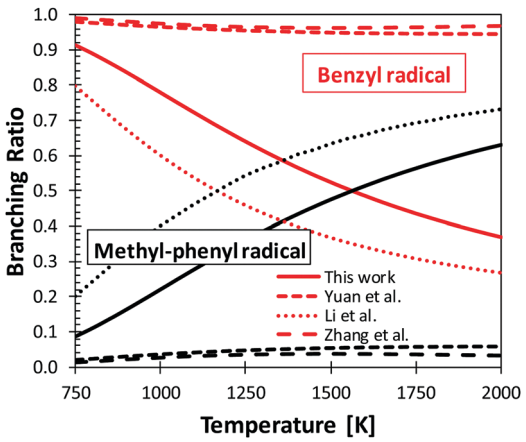

Fig. 9 Branching ratio between benzyl radical (red lines) and methyl-phenyl radical (black lines) for the $O(^3P)$ + toluene H-abstraction channels, according to this study and others from the literature.[2–4,44]

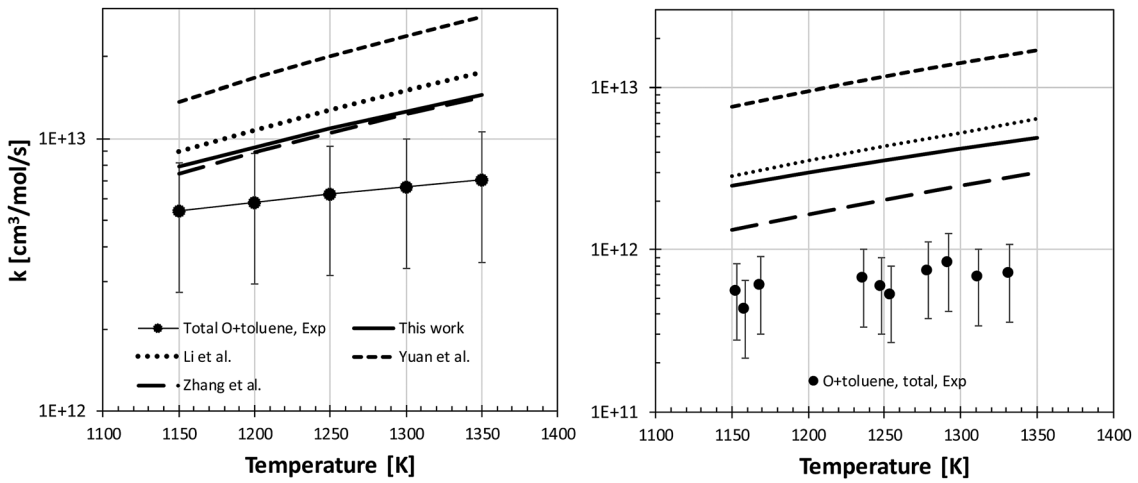

Fig. 8 Comparison between experimental measurements by Hoffmann *et al.*[85] (symbols) for the total rate constant of O + toluene (left panel) and for the H-abstraction by O (right panel). Rate constants for O addition reactions based on analogy with O + benzene.

more relevant and the formation of benzyl radical dominates only up to ~1150 K.

3.1.5 H-Abstractions by $^3O_2$. The recent interest in improving our understanding of the oxidation of alkenes and aromatics[45,87,88] as components of real fuel surrogates pointed at H-abstractions by $^3O_2$ from allylic/benzylic sites as highly sensitive reactions. The sensitivity analyses of Fig. 3 and 4 confirmed these observations, while also highlighting the strong dependence on temperature of the sensitivity coefficients due to the endothermicity of this reaction class, as already discussed in Section 1.2. Very recently Zhou *et al.*[45] systematically studied H-abstraction by $^3O_2$ from structural variants of allylic H-atom sites with an approach similar to that adopted in our study; providing a valuable set of internally consistent barrier heights and rate constants. The H-abstraction of the benzylic H-atom in toluene was also considered. Geometry optimizations and frequency determinations were carried out with the M06-2X functional for a 6-311++G(d,p) basis set. Single-point energy calculations were performed using explicitly correlated coupled cluster energies determined at the CCSD(T)-F12a/cc-pVTZ-F12 level. The barrier height for the reference $C_3H_6 + {}^3O_2$ reaction was also evaluated at the QCISD(T) level, using an extrapolated complete basis set, and with the accurate W1BD method. Additional benchmark calculations were performed at the UCCSD(T)/cc-pVTZ level; with extrapolation to the complete basis set limit using aug-cc-pVQZ and aug-cc-pV5Z basis sets. The computed rate constants were compared with the few experimental measurements available, and showed some deviations especially for the toluene case.

Fig. 10 shows our calculated potential energy surface for the $^3O_2 + C_6H_5CH_3$ system. No evidence of a clear maximum in the potential energy surface is found, as expected from the endothermicity of the reaction. The benzyl radical + HO_2 products lie ~40.5 kcal mol^{-1} above the reactants, while endothermicities of ~60 kcal mol^{-1} are found for the methylphenyl isomers. Transition states are found at ~0.7 kcal mol^{-1} and ~6.7–7 kcal mol^{-1} below the energy of the corresponding products, respectively. These values are consistent with those calculated by Altarawneh *et al.*[89] for the same type of reaction in ethylbenzene. Notably, the energy of the van der Waals well on the product side for H-abstraction from the ring lies above that of the saddle point. This is due to the change in ZPE between saddle point and product complex, which increases by about 1.9 kcal mol^{-1}, while the electronic energy only slightly decreases. This behavior leads to a significant variational effect for this reaction channel, which causes a decrease of the rate constant with respect to the conventional TST value by a factor comprised between 15 and 3 going from 300 K to 2500 K.

Fig. 11a compares the rate constant from this study with the experimental measurements of Eng *et al.*[90] and of Oehlschlaeger *et al.*[29] evidencing large discrepancies (factor of ~10). Our results agree with those reported by Zhou *et al.*[45] to within a factor of ~1.3 in the temperature range for which experimental data are available. For comparison purposes we also report the rate constant calculated by Zhou *et al.*[45] for other primary allylic sites as iso-C_4H_8 ($A \times 0.5$) and $C_3H_6 + {}^3O_2$. The rate constant for H-abstraction from the ring was also computed, and the relative branching ratio as a function of temperature is provided in Fig. 11b. In this case benzyl radical dominates over the whole temperature range of interest, and the formation of methylphenyl radicals only takes place at conditions where most O_2 is consumed by the branching reaction H + O_2 = O + OH.

Zhou *et al.*[45] extensively discussed possible sources of discrepancies with the shock tube measurements of Oehlschlaeger.[29] In typical shock tubes determinations, the accuracy of the

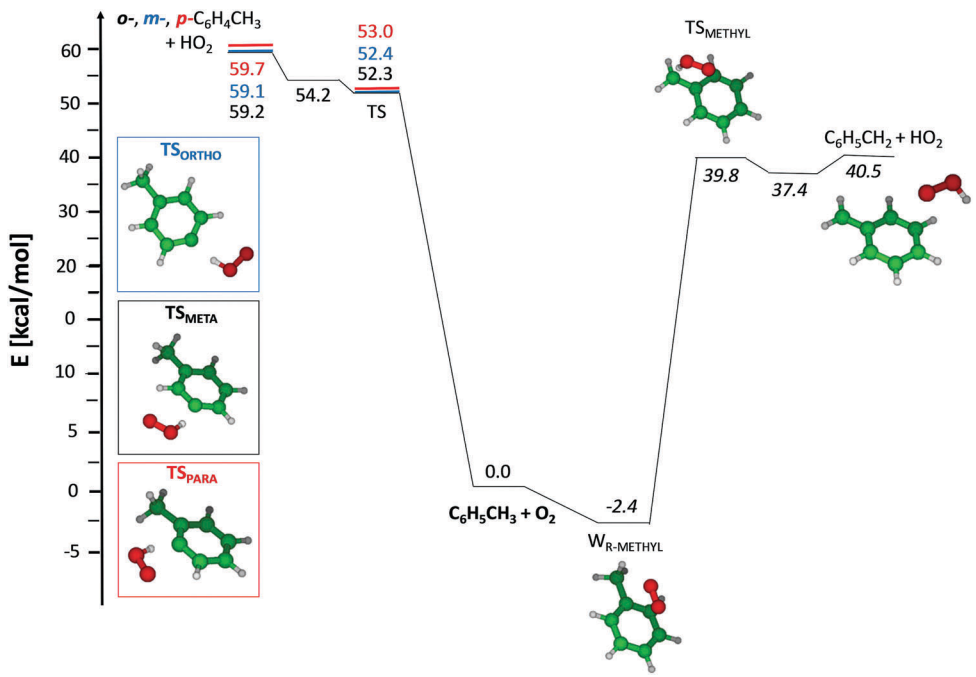

Fig. 10 Potential energy surface for the $^3O_2$ + toluene reaction. Energies in kcal mol^{-1} are relative to the reactants.

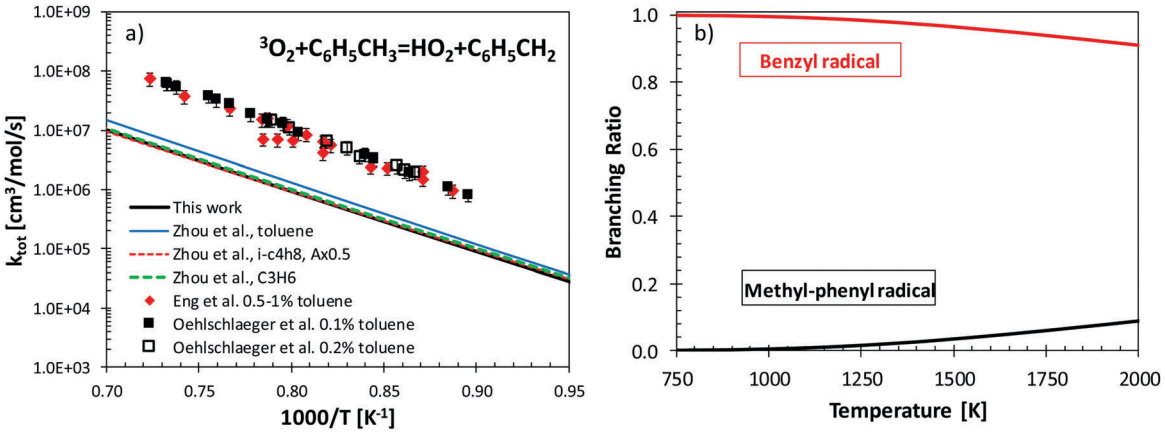

Fig. 11 (a) Comparison of the rate constant of $^3O_2$ + $C_6H_5CH_3$ = HO_2 + $C_6H_5CH_2$ from this and Zhou *et al.*[45] with experimental measurements.[29,90] (b) Branching ratio between benzyl radical and methyl-phenyl radicals.

derived rate constant directly depends on the kinetic model used to interpret the measured absorption. In this case the measured profiles were those of benzyl radical. However, it was observed[45] that the inclusion of the rate suggested by Oehlschlaeger *et al.*[29] in the recent model from Zhang allows to match the benzyl profile quite accurately. Conversely, the introduction of the rate constants calculated in this work, or in Zhou *et al.*, results in a consistent underestimation of benzyl profiles, thus confirming the adequacy of the kinetic model used to fit the experimental data and derive the rate constant. Nevertheless, as discussed in Section 1 in the motivation for our work and in recent studies,[2–4] it must be emphasized that the complexity of toluene combustion kinetics may introduce some additional uncertainty, perhaps due to important unknown or poorly assessed reaction pathways. Moreover, impurities might strongly affect shock tube measurements. This is particularly the case for measurements of H-abstractions by O_2, where very low levels (~0.1–1 ppm) can strongly impact the overall reactivity due to the branching reaction H + O_2 = OH + H.[91] However, the disagreement between experimental measurements and theoretical predictions for this system suggests that further experimental and theoretical studies should be dedicated to the investigation of this important reaction pathway.

3.2 Benzyl radical addition to $^3O_2$

Only a few studies in the literature examine the addition of oxygen to benzyl. Murakami *et al.*[38] investigated the $C_6H_5CH_2$ + $^3O_2$ potential energy surface at the CBS-QB3 level of theory. The rate constant for the dissociation reaction $C_6H_5CH_2OO$ = $C_6H_5CH_2$ + $^3O_2$ was calculated and used to obtain the reverse addition reaction rate constant from thermochemistry. Three different dissociation channels were found for the benzylperoxy radical. The first one leads to the formation of benzaldehyde and OH, the second gives the phenoxy radical and formaldehyde, and the third produces the hydroxyphenyl radical and, again, formaldehyde. A single well master equation analysis was performed at various pressures and temperatures for the backward dissociation and the isomerization channels. Uncertainties in the calculated energies and in the hindered rotation treatment were identified as possible reasons for the observed deviations from experimental measurements of the $C_6H_5CH_2$ + $^3O_2$ = $C_6H_5CH_2OO$ rate constant. An overall branching ratio of 0.7 was calculated for the benzaldehyde + OH channel, in agreement with previous suggestions of Clothier *et al.*[92]

Canneaux *et al.*[93] studied the isomerization channel leading to benzaldehyde and OH. After testing 54 different levels of theory, coupling different methods with different basis sets, they identified CASPT2/ANO-L-VDZP//B3LYP/cc-pVDZ as the best method for reproducing the indirect experimental measurements of Ellis *et al.*[94] at 773 K; claiming a strong multi-reference character of the transition state (TS1 of Fig. 12). The CASPT2 calculations were carried out using a minimal 3 electrons 3 orbitals active space.

Both the works of Murakami *et al.*[38] and of Canneaux *et al.*[93] provide only a limited accuracy description of this important reaction channel, due to both the relatively low level at which the energies were computed and the limited extent of the master equation calculations. In addition, the availability of a recent VRC-TST estimate of the entrance channel rate[48] provides the possibility to compute temperature and pressure dependent rate constants for this channel at a higher level of theory than previously available in the literature. The reaction mechanism we used in this work is shown in Fig. 12. The starting point for its construction was the reaction network proposed by Murakami *et al.*, which was re-examined searching for alternative reaction pathways. It was found that the formation of a five membered ring through cyclization of W1 to W2 through TS3, which can then decompose through TS4 and TS6 to form C_6H_5 and CH_2O, is competitive with the other reaction pathways. Thus, it was included in the final PES used to perform the master equation simulations.

The PES used in the ME simulations is reported in Fig. 13. It is to be noted that it does not contain all the pathways that were examined, but only those that contributed significantly to the system reactivity. The PES is accessed from the addition of O_2 to benzyl through W1.

The calculated exothermicity of the entrance channel is 20.8 kcal mol^{-1}, which is in good agreement with the experimental

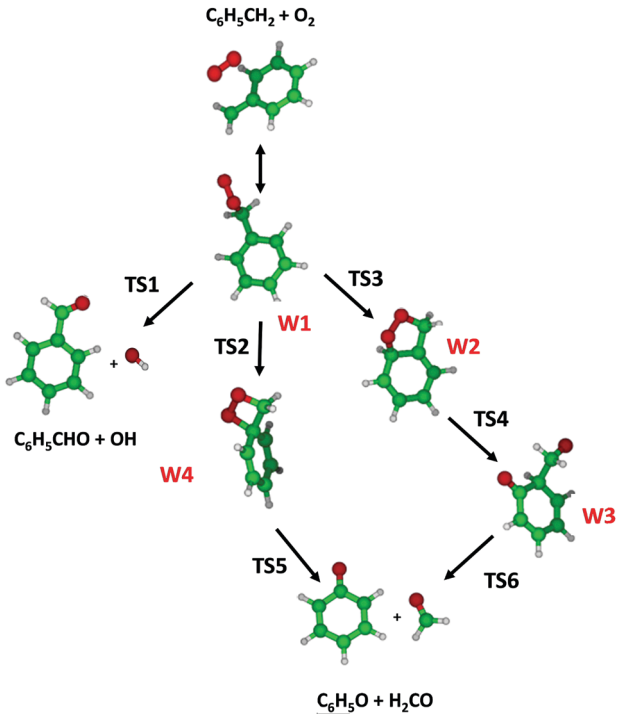

Fig. 12 Investigated reaction pathways on the potential energy surface for the $C_6H_5CH_2 + O_2$ system. Molecular structures represent reactants, wells and products.

values of Elmaimouni[95] (20.0 kcal mol^{-1}) and Fenter *et al.*[96] (21.8 kcal mol^{-1}). The strongly coupled rotations of the $-CH_2OO$ group of W1 (Fig. 14), were treated as a 2-dimensional rotor determining the 2D rotational PES at the B3LYP/CBSB7 level. Potential energy scans are reported in Fig. 14.

Fig. 13 also shows results obtained by Murakami *et al.*[38] at the CBS-QB3 level. The two predictions for the transition state energies are seen to deviate by 1–3 kcal mol^{-1}. As proposed by Murakami *et al.*[38] the most important exit channels are: decomposition to benzaldehyde and OH and decomposition to the phenoxy radical and formaldehyde. The rate of the two pathways is determined in the first case by the rate of TS1 and in the second by TS4 and TS5, which act as rate determining steps for their reaction channels. As these transition states are tight and have a very similar density of states, the branching between the respective reaction channels is controlled mostly by the height of the energy barriers. The TS1 energy barrier is seen to be about 2 kcal mol^{-1} smaller than those of TS4 and TS5, so that the former pathway will be favored over the other two.

It should be mentioned that for O_2 addition to radicals multireference effects may be important for various aspects of the PES describing subsequent isomerizations and dissociations, as is for example the case for O_2 addition to C_2H_3.[97] This may have an important impact on the accurate estimation of the PES energetics. The coupled cluster T1 diagnostics reported in Table 4 provide some indication regarding the expected level of multireference character in the wave function. For an open shell system, when T1 > 0.03 it may become necessary to use a multi-reference approach to confirm the accuracy of the energies determined with a single reference method. Both TS4 and TS6 transition states, which belong to the same reaction pathway, are seen to exhibit a significant multireference character.

To investigate this aspect, the saddle point of TS4 was searched at the CASPT2/cc-pVDZ level with a minimal (3e,3o) active space; unfortunately without success. Single point energy calculations at the RHF/cc-pVDZ and CCSD(T)/cc-pVDZ levels along the M06-2X/6-311++G(d,p) IRC path, using a wave function

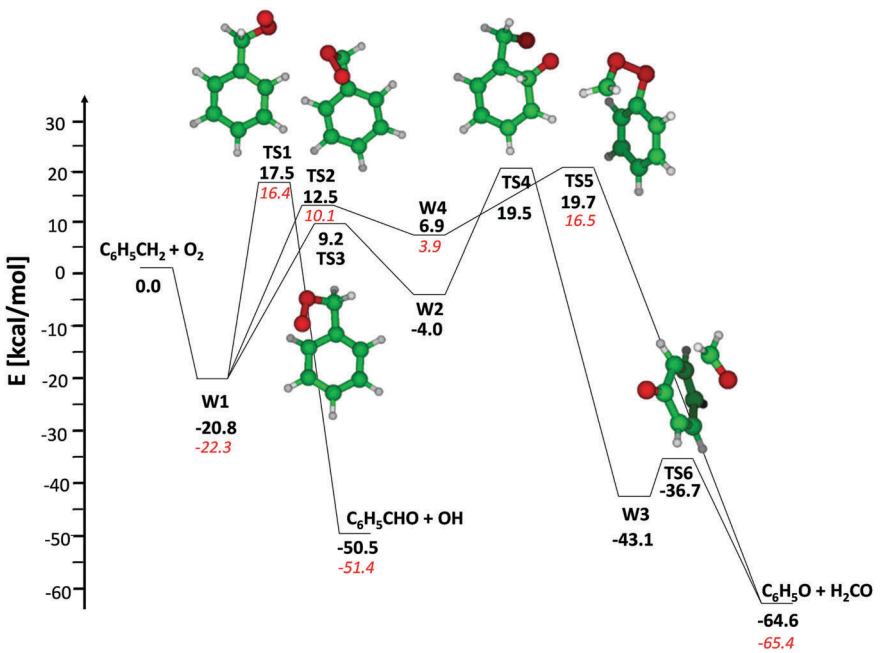

Fig. 13 Potential energy surface for the $C_6H_5CH_2 + O_2$ reaction. Numbers in red italics are CBS-QB3 calculated energies from Murakami *et al.*[38] Numbers in black are energies computed in this study. Molecular structures represent transition states.

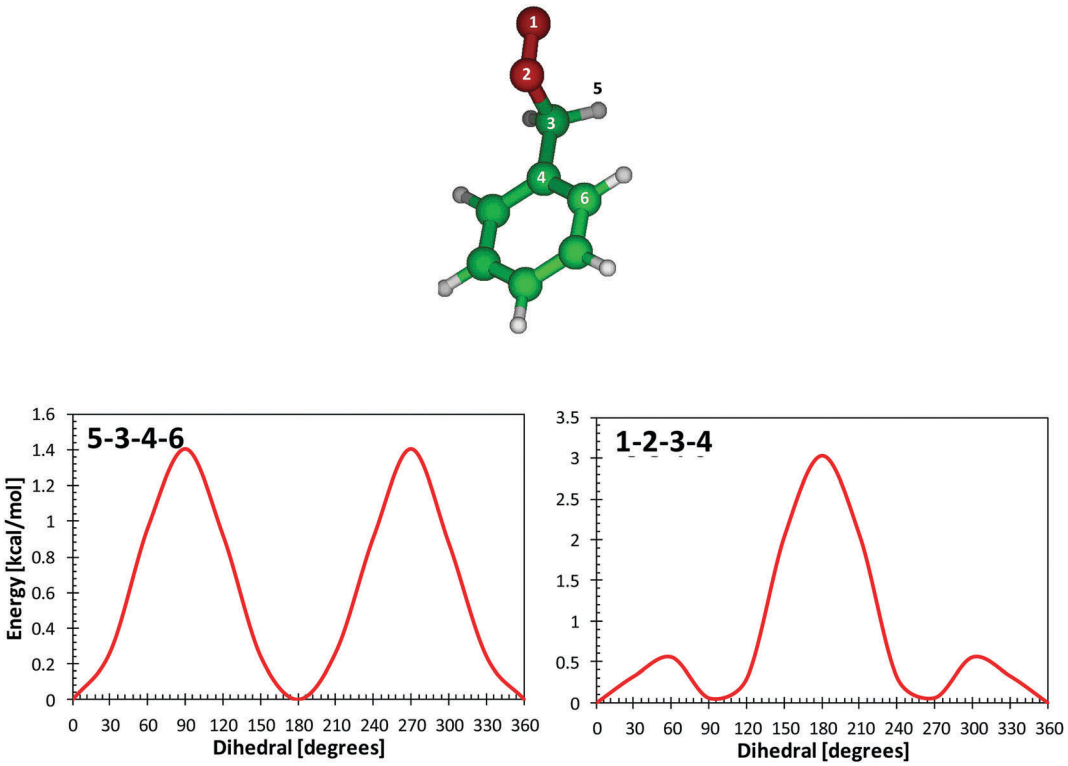

Fig. 14 W1 minimum energy structure as determined at the B3LYP/CBSB7 level. Dihedral scan of the coupled rotations of CH_2–OO at the B3LYP/CBSB7 level.

Table 4 T1 diagnostics calculated at the CCSD(T)-F12/VTZ-F12 level[64,65]

	TS1	TS2	TS3	TS4	TS5	TS6
T1-diagnostic	0.024	0.019	0.020	0.034	0.017	0.038

determined from the reactant and the product side as a guess, produced very different potential energy surfaces, as highlighted in Fig. S5 of the ESI.† This is often indicative of a strong multireference character of the investigated reaction. Despite a systematic increase of the active space, we were not able to locate a saddle point at the CASPT2 level. We attribute this failure to the relatively limited size of the active space we were able to use for the calculations, which probably would have required the inclusion of all six π electrons of the benzyl ring and the eight 2p electrons on the involved oxygen atoms. Unfortunately, such calculations were too computationally expensive, even when using a limited basis set. It can therefore be concluded that there remains considerable uncertainty in the energy of TS4.

Fig. 15a reports the calculated rate constants for the entrance channel ($C_6H_5CH_2 + O_2 = C_6H_5CH_2OO$) as a function of temperature and pressure. The calculated high pressure limit (solid black line) shows a slightly positive temperature dependence, in contrast with what was reported previously[38] by Murakami *et al.*,[38] who found a positive dependence for $T < 550$ K and a negative non-monotonic dependence for $T > 550$ K. Between 300 and 400 K the high pressure limit calculated in this study is a factor of ∼4 higher and correctly reproduces the experimental measurements within their uncertainties.

Benzyl peroxy radical decomposition rate constants are plotted in Fig. 15b. As an example, a typical high pressure limit decomposition rate constant of an alkyl-peroxy radical is also reported (green line).[46] While in alkanes the peroxy-radicals can easily undergo successive isomerizations and low temperature branching pathways, the relatively unstable benzyl-peroxy radical more likely decomposes back to the reactants, partially explaining the high anti-knocking properties of toluene.

Fig. 15c shows the equilibrium constant calculated in this study (black line) and that reported by Murakami *et al.*[38] (red line). Despite a factor of ∼5 deviation from the experimental measurements of Fenter *et al.*,[96] K_{eq} calculated in this study better reproduces the temperature dependence, highlighting a lower stability of $C_6H_5CH_2OO^\bullet$ compared to Murakami *et al.*[38]

The rate constants for the decomposition channels of $C_6H_5CH_2OO^\bullet$ are orders of magnitude lower than that for the backward dissociation to reactants, which is thus the main reaction channel for this system. The dominant reaction channel for all the conditions here examined is the well-skipping reaction between O_2 and benzyl to form benzaldehyde and ·OH. The branching between the benzaldehyde + OH and the phenoxy + H_2CO channels is reported in Fig. 16 for T = 600–1500 K, and p = 10 atm. The high branching to benzaldehyde (∼0.87–0.96) calculated for all the examined conditions increases toluene reactivity, as it converts a resonantly stabilized radical (benzyl) and molecular oxygen into reactive $^\bullet$OH.

Table S3 of the ESI† provides the calculated rate constants, together with fitting temperature ranges, for direct use in

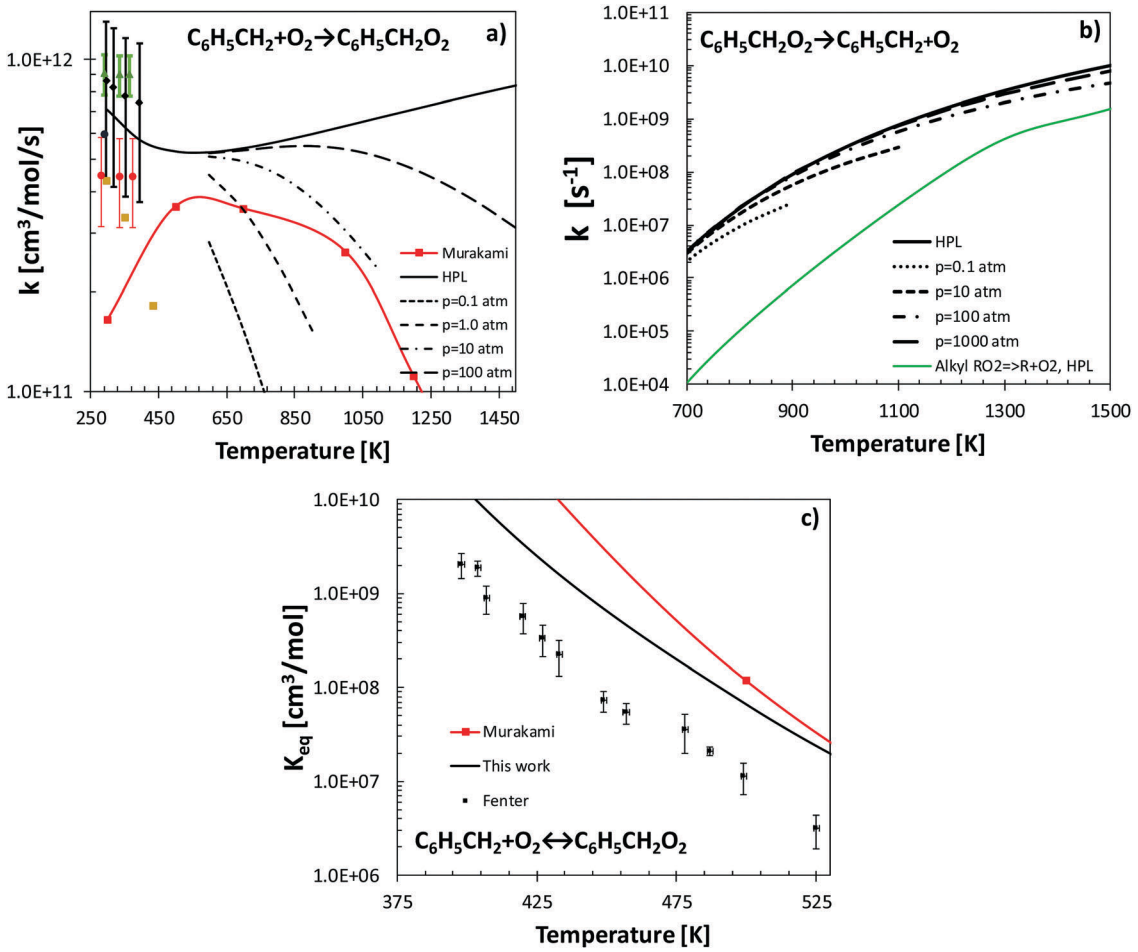

Fig. 15 (a) Calculated $k(T,p)$ rate constants for benzyl addition to O_2 from this study (black lines), high pressure limit (HPL) from Murakami *et al.*[9] (red line) and comparison with experimental data.[95,96,98,99] (b) Calculated $k(T,p)$ rate constants for benzyl-peroxy radical decomposition: black lines: this study, green line: typical decomposition rate constant of an alkyl peroxy radical. (c) Comparison of calculated equilibrium constant with experimental data of Fenter *et al.*[96] and Murakami *et al.*[38] (red line).

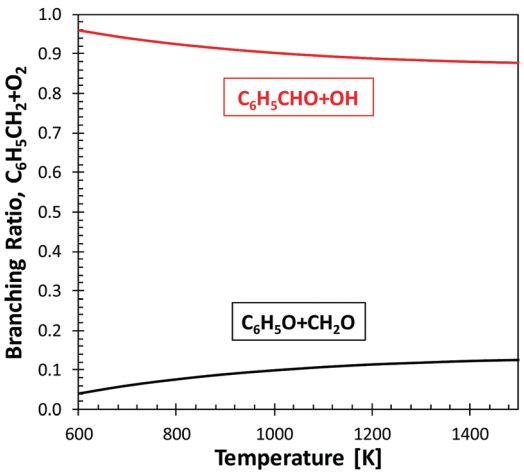

Fig. 16 Temperature dependence of the calculated product branching ratios forming benzaldehyde and OH or phenoxy radical and formaldehyde. p = 0.1 atm.

chemical kinetic mechanisms for toluene oxidation. The reported rates are either high pressure limits or were fitted in temperature ranges that vary with pressure depending on the possibility to form one or more thermodynamically stable energy wells. Of the considered energy wells, the one that is more easily formed is W1, the benzyl-peroxy radical. The temperature below which W1 is thermodynamically stable increases with pressure from 800 K at 1 atm to 2100 K at 1000 atm.

4. Implications to kinetic modelling of toluene oxidation

This section aims at guiding further improvements and updates of literature toluene kinetic models, by discussing the impact of different sets of rate constants, including those calculated in this study, on POLIMI model predictions. Only a subset of the full set of validation targets reported in the ESI† is discussed in the following, with the aim of covering a wide and significant range of operating conditions.

Fig. 17 shows the effect of different rate constants for H-abstractions by OH radical. Generally, the adoption of the rate constants suggested by Li *et al.*[44] lead to an increased reactivity,

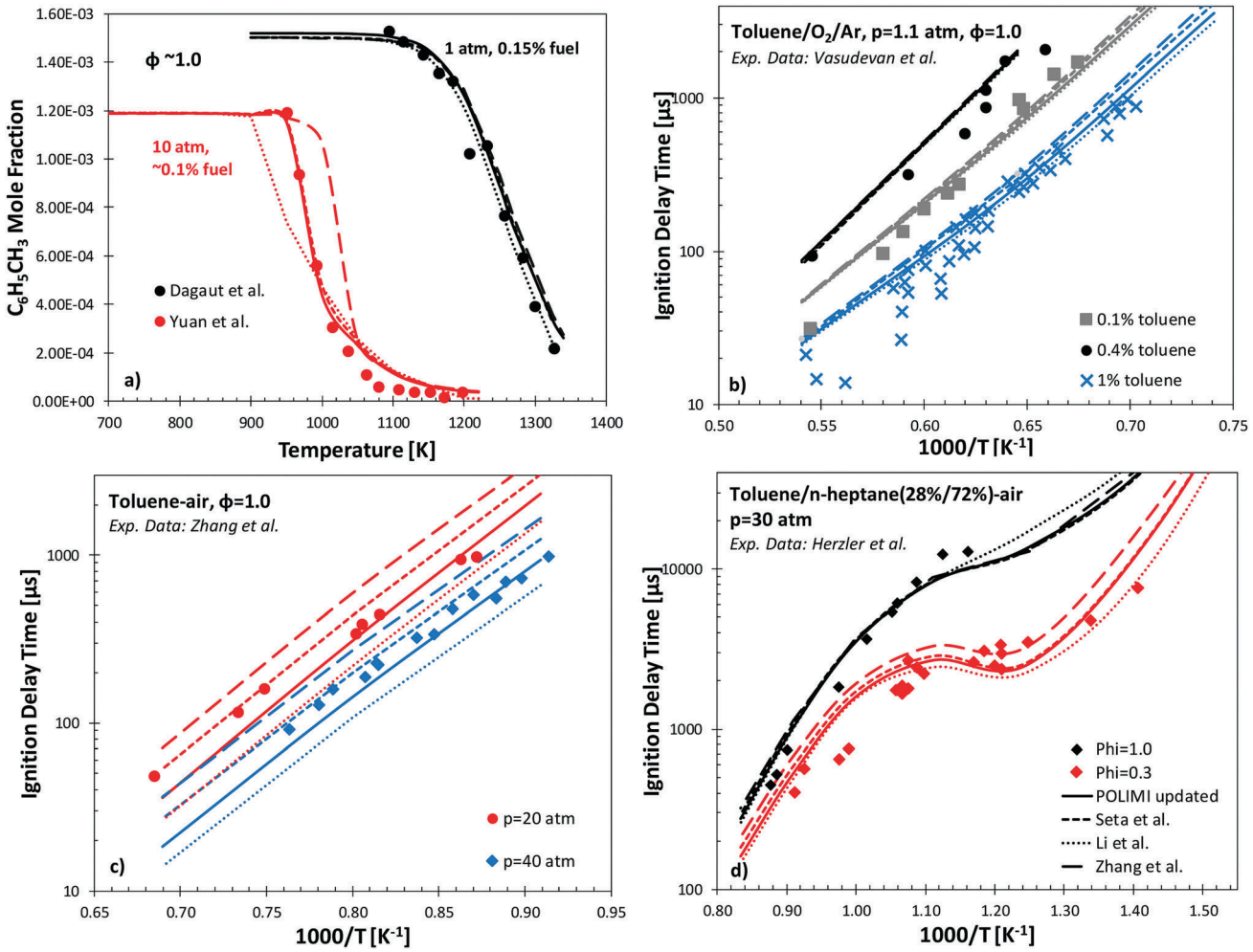

Fig. 17 Effect of rate constants for H-abstractions by OH from this study (solid lines), Seta *et al.*[27] (dashed lines), Li *et al.*[44] (dotted lines), Zhang *et al.* (long dashed lines).[4] Experimental data (symbols) from ref. 2, 4, 10, 12 and 14.

due to higher yields of methyl phenyl radicals. Conversely, the modified rate constants from Seta *et al.*,[27] which are included in the Zhang *et al.* mechanism,[4] inhibit reactivity. As clearly discussed by the authors, in fact, while maintaining the same total rate constant recommended by Seta *et al.*,[27] it was necessary to further increase the formation of benzyl radical and decrease the formation of methyl phenyl radical to improve agreement with experimental data. As discussed in Section 3.1.1, the rate constants calculated in our work agree very well with the recommendation of Seta *et al.*,[27] both in terms of absolute value and relative branching fractions. As a result, there is a more limited impact on reactivity represented by the solid and short-dashed lines in Fig. 17.

For low pressure high temperature conditions the impact is limited, as expected from the lower sensitivity coefficients discussed in Section 1. Variations on the order of ~10% are observed for fuel conversion in the JSR case at 1 atm (Fig. 17a) and ~10–20% variation in terms of atmospheric pressure ignition delay times (Fig. 17b). The higher pressure and lower temperature JSR case shows instead the significant effect of different branching fractions (Fig. 5b). On one hand it is possible to observe the enhanced reactivity obtained with the recommendation from Li *et al.*,[44] favoring methyl phenyl and leading to an ~30–40 K anticipation in reactivity. On the other hand, the optimized rates from Zhang *et al.*[4] favor benzyl radical, delaying toluene reactivity by ~40–50 K. High pressure ignition delay times are very sensitive to H-abstractions by OH, which results in the large impact observed in Fig. 17c, with variations of up to a factor of ~3. When including the rate parameters from Li *et al.*, ignition delay times decrease by a factor of ~1.5. Variations of the same order of magnitude, but in the opposite directions are obtained with the values of Seta *et al.*,[27] and up to a factor of ~2 in the case of Zhang.

Fig. 17d reports ignition delay time data for a toluene/n-heptane mixture (28/72 mol%) representative of a RON = 84 and MON = 73 gasoline.[14] This last case was selected to investigate the impact on surrogate mixtures emulating real fuels, and mostly to allow better insight into toluene kinetics at lower temperatures. In fact, similarly to DME in the study of Zhang *et al.*,[4] *n*-heptane acts as a radical initiator and its sub-mechanism was recently updated in the POLIMI kinetic framework.[100] Also in this case, the effect is quite significant, in particular for the

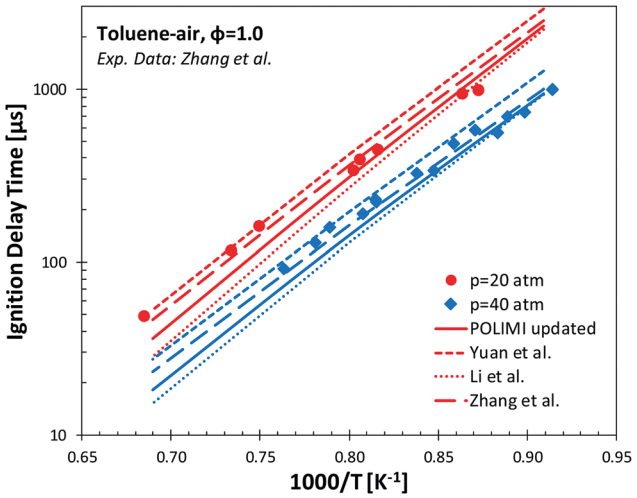

Fig. 18 Effect of rate constants for H-abstractions by $O(^3P)$ from this study (solid lines), from Li *et al.*[44] (dotted lines), and from recent toluene kinetic models.[2–4] Experimental data (symbols) from ref. 4.

leaner case and moving towards lower temperatures. Indeed, the low temperature reactivity of *n*-heptane provides high yields of OH radicals resulting in the high sensitivity of ignition delay times to toluene H-abstraction rate constants.

H-Abstractions by $O(^3P)$ are also found to greatly affect high pressure ignition delay times at high-intermediate temperatures. Fig. 18 shows the enhancing effect derived from the inclusion of the rate constants suggested by Li *et al.*,[44] leading to a decrease in ignition delay times by a factor of ~1.3. The model of Zhang *et al.*[4] implements the rate constants suggested by Narayanaswamy *et al.*,[101] strongly favoring benzyl radical formation over methylphenyl (Fig. 9). Indeed, the inclusion of such rates increases the ignition delay times by ~20–30%. Yuan *et al.*[2,3] adopted the rate constant suggested by Bounaceur *et al.*[9] for the methyl phenyl channel, and based their estimate on analogy with CH_4 + O for the benzyl radical formation channel. These parameters also lead to a large predominance of benzyl radical, and due to a higher total rate of H-abstraction (Fig. 8) the ignition times increase even further.

For both the O + $C_6H_5CH_3$ and the OH + $C_6H_5CH_3$ pathways, addition and *ipso*-substitution reaction channels are expected

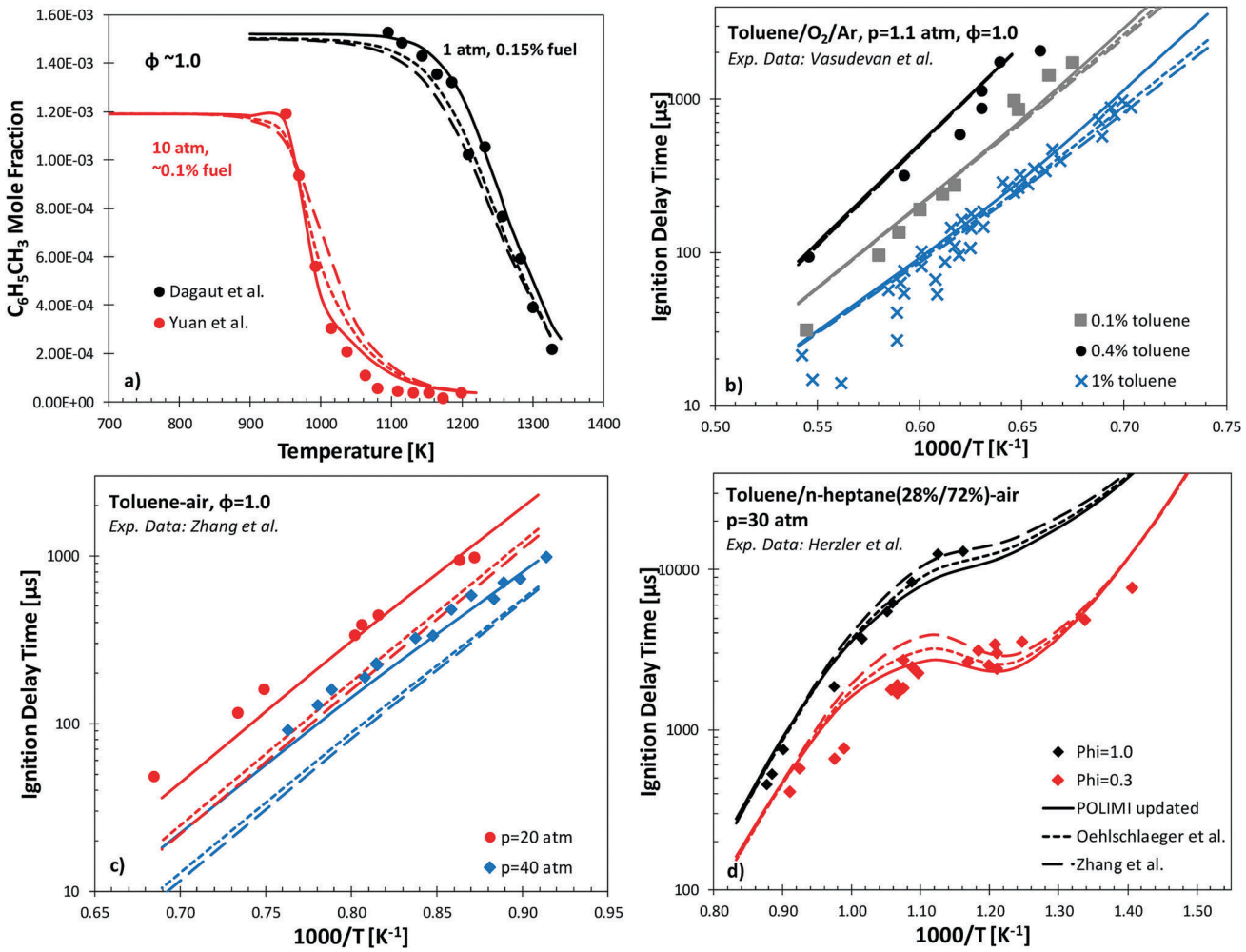

Fig. 19 Effect of rate constants for H-abstractions by O_2 from this study (solid lines), from Oehlschlaeger *et al.*[29] (dashed lines), and the modified rate constant in Zhang *et al.* (long dashed lines).[4] Experimental data (symbols) from ref. 2, 4, 10 and 12.

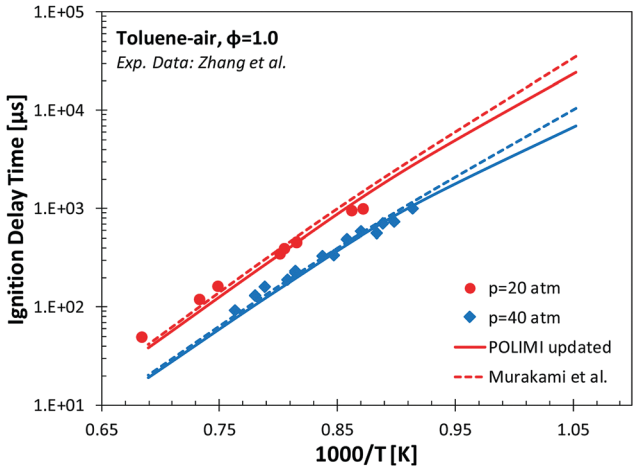

Fig. 20 Effect of rate constants for O_2 + benzyl radical from this study (solid lines), and from Murakami *et al.*[38] Experimental data (symbols) from ref. 4.

to be relevant, in particular at lower temperatures. Experimental measurements of these channels have been reported in the literature, under quite limited temperature and pressure ranges, as discussed in previous sections. However, a systematic theoretical investigation able to extend such observations at conditions more relevant for combustion kinetic models validation is still missing from the literature, mostly due to the intrinsic complexity of potential energy surfaces involving an O/OH addition to an aromatic ring.

Fig. 19 shows the impact on POLIMI model predictions of different rate constants for the H-abstraction by molecular oxygen. Zhang *et al.*[4] increased the rate constant proposed by Oehlschlaeger *et al.*[29] by a factor of 2, resulting in a factor of ~20 difference with the more recent estimate from Zhou *et al.*[45] and that from this work. The endothermic nature of such channels results in an opposite effect depending on temperature, as clearly showed for the JSR cases in Fig. 19a. For $T > 1100$ K, the reaction acts as an initiation step, while at lower temperatures, the reaction terminates the radical chain driving a reduction in reactivity. Low pressure high temperature ignition delay times (Fig. 19b) decrease up to a factor ~2 at lower temperatures and for the higher toluene concentration (1%). Similar enhancing effects are obtained for the toluene/air high pressure cases

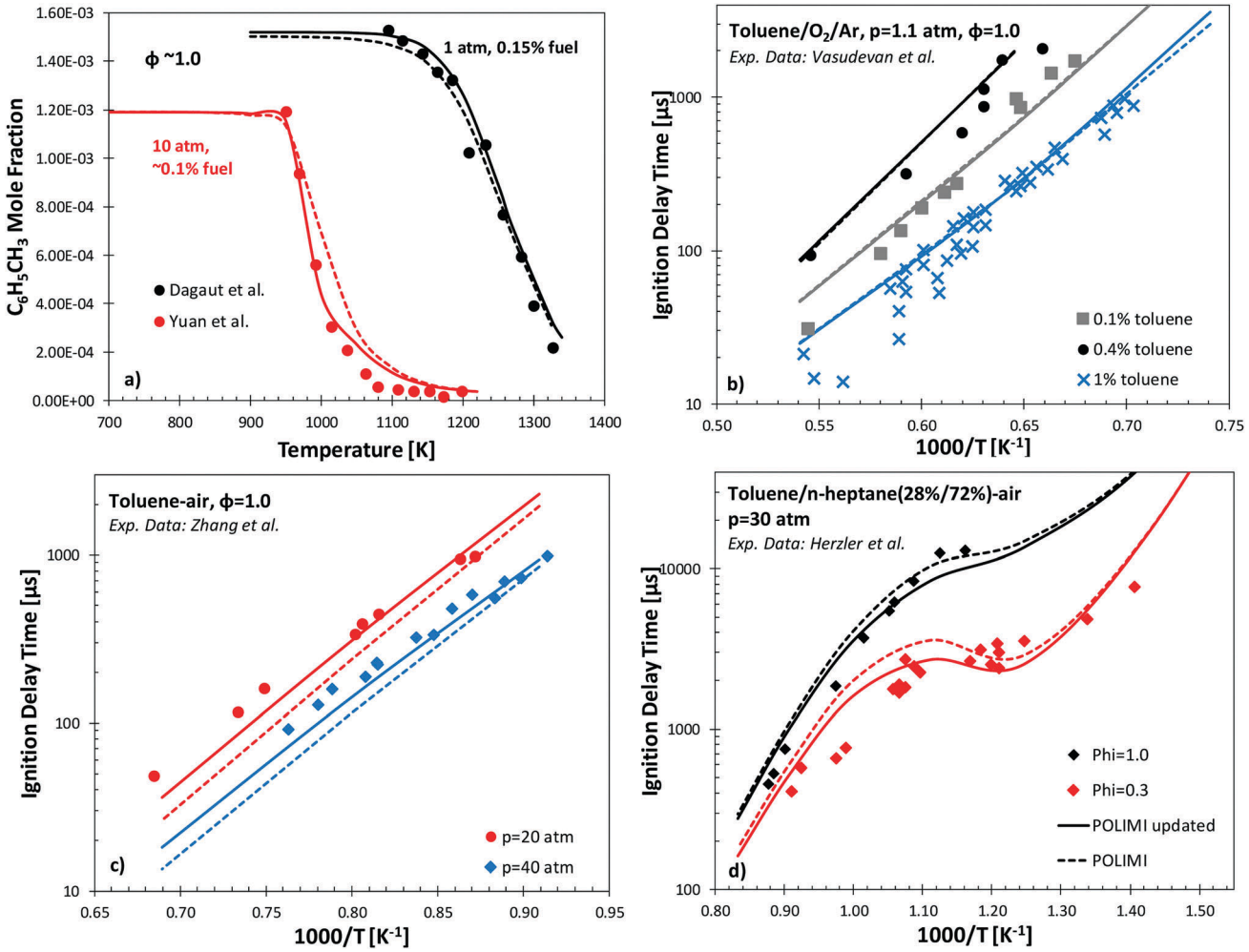

Fig. 21 Global effect of rate constants calculated in this study. Experimental data (symbols) from ref. 2, 4, 10 and 12, simulation results lines: starting POLIMI mechanism (dashed) and POLIMI updated with rate constants from this study (solid).

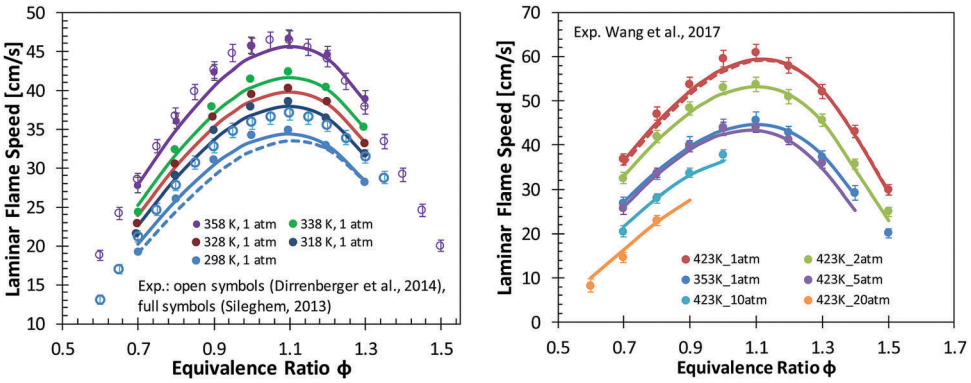

Fig. 22 Experimental (symbols)[36–42] and simulated (lines) laminar flame speeds of toluene at different pressures and initial temperatures.

of Fig. 19c. The inhibition effect at lower temperature is clearly represented in Fig. 19d for the toluene/n-heptane mixture.

The theoretical investigation of the potential energy surface of $C_6H_5CH_2 + O_2$, was discussed in Section 3.2. Electronic structure and energy calculations for reactants, wells, transition states and products have been performed at, possibly, the most accurate level of theory affordable for a 9 heavy atoms system. The master equation analysis provided rate constants as a function of temperature and pressure for direct use in existing chemical kinetic mechanisms. Fig. 20 shows the impact of the rate constants calculated by Murakami and those calculated in this work on POLIMI model predictions. Murakami *et al.*,[38] predicted a significant stabilization of the peroxy radical (Fig. 15c), with successive decomposition to benzaldehyde and OH or phenoxy radical and formaldehyde. Meanwhile, according to our results the bimolecular reaction $C_6H_5CH_2 + O_2 = C_6H_5CHO + OH$ plays the dominant role and significantly promotes reactivity. Variations in terms of ignition delay times are within ~20% in the temperature range of the measurements of Zhang *et al.*[4] increasing up to ~40% at $T = 950$ K.

5. Conclusions

This work presents the theoretical investigation of key reaction pathways in toluene oxidation. Starting from previous versions of the POLIMI kinetic model,[22,26] an updated version was produced based on theoretical and experimental determinations of rate constants,[27–44] and on recently developed toluene kinetic models.[2–4] Moreover, in the attempt to converge to a community standard base chemistry and to closely focus on specific fuel chemistry, the C0–C3 mechanism of the POLIMI model was updated including the modules from National University of Ireland, Galway.[50–53]

Sensitivity analysis for the updated POLIMI model highlighted important reaction pathways still carrying uncertainties. Within those, H-abstractions by OH, $O(^3P)$, HO_2 and $^3O_2$ together with the interactions between molecular oxygen and benzyl radical ($C_6H_5CH_2$) were found to be relevant for accurately predicting toluene oxidation. The rate constants for these H-abstraction reactions were investigated using electronic structure calculations and transition state theory in its conventional and variational formulations. Temperature and pressure dependent rate coefficients for the $O_2 + C_6H_5CH_2$ channels were investigated using variable reaction coordinate transition state theory (VRC-TST) and the master equation, thereby unravelling the dominant role of the direct bimolecular channel forming benzaldehyde and OH. Implications to kinetic modelling of the new rate parameters are also discussed, thereby encouraging and guiding updates of existing models.

Fig. 21 and 22 shows the effect of the rate coefficients calculated in this work on the starting POLIMI model. Overall, the impact seems to be more limited compared to the discussion in Section 4. This result is due to the counterbalancing effects of the different updated rate constants. However, the updated POLIMI model better predicts the experimental measurements of toluene oxidation in JSR at 10 atm (Fig. 21a) and high pressure ignition delay times of both neat toluene and a gasoline surrogate, as reported in Fig. 21c and d, respectively. Smaller variations are observed for the lower pressure cases, both in JSR and shock tubes.

Fig. 22 compares POLIMI model predictions with laminar flame speed measurements from the literature.[18,19,102] In particular, simulations for the atmospheric pressure cases at 298 K and 423 K unburned gas temperatures have been performed with the two versions of the mechanism. For this case, improved agreement is again obtained with the latest version of the kinetic model.

The rate constants determined in this work are appropriate for direct use in chemical kinetic models and advance the knowledge on toluene oxidation. This work also underlines both the need for more detailed experimental data at lower temperatures and encourages theoretical assessments of other reaction channels:

- $HO_2 + C_6H_5CH_2$ investigated by da Silva and co-workers[39–43] still plays a dominant role. Up-to-date theoretical methods together with the multi-well master equation can provide pressure and temperature dependent rate constants of higher accuracy compared to the previous studies. The same applies to interactions of molecular oxygen with methyl-phenyl radicals;
- Recombination pathways involving benzyl and other C7 radicals, together with methyl still present large uncertainties.

Not only toluene models, but also PAH and soot growth mechanisms would benefit from a better assessment of these channels;

• Interactions of stable benzyl radical with other intermediate species (benzaldehyde, cresol, benzene, cyclopentadiene *etc.*) are relevant and can compete with the above recombination channels;

• Interactions of O/OH and O_2 with the aromatic ring *via* addition and *ipso*-substitution reactions also lack a systematic investigation. Similarity and analogy rules would also allow for an extension of the predicted outcomes to PAH and soot oxidation mechanisms;

• Oxidation of key intermediates (phenol, cresol, benzaldehyde *etc.*) have only been marginally addressed in the literature. Wide ranging experimental studies together with theoretical investigation are necessary to improve the reliability of important subsets in toluene oxidation.

Conflicts of interest

There are no conflicts to declare.

Acknowledgements

Dr Matteo Pelucchi acknowledges the support of Argonne National Laboratory visiting graduate program. Prof. Carlo Cavallotti acknowledges the support of the Chemical Sciences and Engineering Division of Argonne National Laboratory for the sabbatical period spent there, during which most of this work was done. The authors gratefully acknowledge Prof. Eliseo Ranzi and Eng. Warumporn Pejpichestakul for helpful discussions and for collaboration in implementing the new core mechanism and in revising MAH chemistry. The authors acknowledge helpful discussions with Dr Raghu Sivaramakrishnan at Argonne National Laboratory and with Dr Kieran Somers, Prof. John Simmie and Prof. H. J. Curran at National University of Ireland, Galway. This material is based in part on work supported by the U.S. Department of Energy, Office of Science, Office of Basic Energy Sciences, Division of Chemical Sciences, Geosciences, and Biosciences under contract no. DE-AC02-06CH11357.

References

1 G. T. Kalghatgi, *Int. J. Engine Res.*, 2014, **15**, 383–398.
2 W. Yuan, Y. Li, P. Dagaut, J. Yang and F. Qi, *Combust. Flame*, 2015, **162**, 3–21.
3 W. Yuan, Y. Li, P. Dagaut, J. Yang and F. Qi, *Combust. Flame*, 2015, **162**, 22–40.
4 Y. Zhang, K. P. Somers, M. Mehl, W. J. Pitz, R. F. Cracknell and H. J. Curran, *Proc. Combust. Inst.*, 2017, **36**, 413–421.
5 A. Burcat, C. Snyder and T. Brabbs, *NASA Tech. Memo.*, 1986, 87312.
6 K. M. Pamidimukkala, R. D. Kern, M. R. Patel, H. C. Wei and J. H. Kiefer, *J. Phys. Chem.*, 1987, **91**, 2148–2154.
7 M. B. Colket and D. J. Seery, *Proc. Combust. Inst.*, 1994, **25**, 883.
8 R. Sivaramakrishnan, R. S. Tranter and K. Brezinsky, *J. Phys. Chem. A*, 2006, **110**, 9388–9399.
9 R. Bounaceur, I. Da Costa, R. Fournet, F. Billaud and F. Battin-Leclerc, *Int. J. Chem. Kinet.*, 2005, **37**, 25–49.
10 P. Dagaut, G. Pengloan and A. Ristori, *Phys. Chem. Chem. Phys.*, 2002, **4**, 1846–1854.
11 G. Pengloan, P. Dagaut, N. Djebaıli-Chaumeix, C. Paillard and M. Cathonnet, *Combustion Institute, French Section*, Orléans, 2001, p. 9.
12 V. Vasudevan, D. Davidson and R. K. Hanson, *Proc. Combust. Inst.*, 2005, **30**, 1155–1163.
13 D. Davidson, B. Gauthier and R. K. Hanson, *Proc. Combust. Inst.*, 2005, **30**, 1175–1182.
14 J. Herzler, M. Fikri, K. Hitzbleck, R. Starke, C. Schulz, P. Roth and G. T. Kalghatgi, *Combust. Flame*, 2007, **149**, 25–31.
15 G. Mittal and C.-J. Sung, *Combust. Flame*, 2007, **150**, 355–368.
16 R. Sivaramakrishnan, R. S. Tranter and K. Brezinsky, *Proc. Combust. Inst.*, 2005, **30**, 1165–1173.
17 R. Sivaramakrishnan, R. S. Tranter and K. Brezinsky, *Combust. Flame*, 2004, **139**, 340–350.
18 P. Dirrenberger, P.-A. Glaude, R. Bounaceur, H. Le Gall, A. P. da Cruz, A. Konnov and F. Battin-Leclerc, *Fuel*, 2014, **115**, 162–169.
19 G. Wang, Y. Li, W. Yuan, Z. Zhou, Y. Wang and Z. Wang, *Combust. Flame*, 2017, **184**, 312–323.
20 K. P. Somers, R. F. Cracknell and H. J. Curran, *European Combustion Meeting*, Budapest, Hungary, 2015.
21 M. Mehl, W. J. Pitz, C. K. Westbrook and H. J. Curran, *Proc. Combust. Inst.*, 2011, **33**, 193–200.
22 E. Ranzi, A. Frassoldati, A. Stagni, M. Pelucchi, A. Cuoci and T. Faravelli, *Int. J. Chem. Kinet.*, 2014, **46**, 512–542.
23 J. C. Andrae, *Fuel*, 2013, **107**, 740–748.
24 J. C. Andrae, T. Brinck and G. T. Kalghatgi, *Combust. Flame*, 2008, **155**, 696–712.
25 A. Cuoci, A. Frassoldati, T. Faravelli and E. Ranzi, *Comput. Phys. Commun.*, 2015, **192**, 237–264.
26 E. Ranzi, A. Frassoldati, R. Grana, A. Cuoci, T. Faravelli, A. P. Kelley and C. K. Law, *Prog. Energy Combust. Sci.*, 2012, **38**, 468–501.
27 T. Seta, M. Nakajima and A. Miyoshi, *J. Phys. Chem. A*, 2006, **110**, 5081–5090.
28 M. A. Oehlschlaeger, D. F. Davidson and R. K. Hanson, *Proc. Combust. Inst.*, 2007, **31**, 211–219.
29 M. A. Oehlschlaeger, D. F. Davidson and R. K. Hanson, *Combust. Flame*, 2006, **147**, 195–208.
30 M. A. Oehlschlaeger, D. F. Davidson and R. K. Hanson, *J. Phys. Chem. A*, 2006, **110**, 9867–9873.
31 R. Sivaramakrishnan and J. V. Michael, *Proc. Combust. Inst.*, 2011, **33**, 225–232.
32 L. B. Harding, S. J. Klippenstein and Y. Georgievskii, *J. Phys. Chem. A*, 2007, **111**, 3789–3801.
33 S. J. Klippenstein, L. B. Harding and Y. Georgievskii, *Proc. Combust. Inst.*, 2007, **31**, 221–229.

34 C. Cavallotti, M. Derudi and R. Rota, *Proc. Combust. Inst.*, 2009, **32**, 115–121.
35 M. Derudi, D. Polino and C. Cavallotti, *Phys. Chem. Chem. Phys.*, 2011, **13**, 21308–21318.
36 D. Polino and C. Cavallotti, *J. Phys. Chem. A*, 2011, **115**, 10281–10289.
37 D. Polino, A. Famulari and C. Cavallotti, *J. Phys. Chem. A*, 2011, **115**, 7928–7936.
38 Y. Murakami, T. Oguchi, K. Hashimoto and Y. Nosaka, *J. Phys. Chem. A*, 2007, **111**, 13200–13208.
39 G. da Silva and J. W. Bozzelli, *Proc. Combust. Inst.*, 2009, **32**, 287–294.
40 G. da Silva and J. W. Bozzelli, *J. Phys. Chem. A*, 2009, **113**, 6979–6986.
41 G. da Silva, C.-C. Chen and J. W. Bozzelli, *J. Phys. Chem. A*, 2007, **111**, 8663–8676.
42 G. da Silva, J. A. Cole and J. W. Bozzelli, *J. Phys. Chem. A*, 2009, **113**, 6111–6120.
43 G. da Silva, M. R. Hamdan and J. W. Bozzelli, *J. Chem. Theory Comput.*, 2009, **5**, 3185–3194.
44 S.-H. Li, J.-J. Guo, R. Li, F. Wang and X.-Y. Li, *J. Phys. Chem. A*, 2016, **120**, 3424–3432.
45 C.-W. Zhou, J. M. Simmie, K. P. Somers, C. F. Goldsmith and H. J. Curran, *J. Phys. Chem. A*, 2017, **121**, 1890–1899.
46 E. Ranzi, M. Dente, A. Goldaniga, G. Bozzano and T. Faravelli, *Prog. Energy Combust. Sci.*, 2001, **27**, 99–139.
47 E. Ranzi, T. Faravelli, P. Gaffuri and A. Sogaro, *Combust. Flame*, 1995, **102**, 179–192.
48 F. Zhang, A. Nicolle, L. Xing and S. J. Klippenstein, *Proc. Combust. Inst.*, 2017, **36**, 169–177.
49 A. Chang, J. W. Bozzelli and A. M. Dean, *Z. Phys. Chem.*, 2000, **214**, 1533.
50 A. Kéromnès, W. K. Metcalfe, K. A. Heufer, N. Donohoe, A. K. Das, C.-J. Sung, J. Herzler, C. Naumann, P. Griebel and O. Mathieu, *Combust. Flame*, 2013, **160**, 995–1011.
51 W. K. Metcalfe, S. M. Burke, S. S. Ahmed and H. J. Curran, *Int. J. Chem. Kinet.*, 2013, **45**, 638–675.
52 S. M. Burke, U. Burke, R. Mc Donagh, O. Mathieu, I. Osorio, C. Keesee, A. Morones, E. L. Petersen, W. Wang and T. A. DeVerter, *Combust. Flame*, 2015, **162**, 296–314.
53 S. M. Burke, W. Metcalfe, O. Herbinet, F. Battin-Leclerc, F. M. Haas, J. Santner, F. L. Dryer and H. J. Curran, *Combust. Flame*, 2014, **161**, 2765–2784.
54 B. Ruscic, *Int. J. Quantum Chem.*, 2014, **114**, 1097–1101.
55 B. Ruscic, R. E. Pinzon, G. Von Laszewski, D. Kodeboyina, A. Burcat, D. Leahy, D. Montoy and A. F. Wagner, *J. Phys.: Conf. Ser.*, 2005, **16**, 561–570.
56 A. Burcat and B. Ruscic, *Third millenium ideal gas and condensed phase thermochemical database for combustion with updates from active thermochemical tables*, Argonne National Laboratory Argonne, IL, 2005.
57 Y. Zhao and D. G. Truhlar, *Theor. Chem. Acc.*, 2008, **120**, 215–241.
58 M. Urban, J. Noga, S. J. Cole and R. J. Bartlett, *J. Chem. Phys.*, 1985, **83**, 4041–4046.
59 R. A. Kendall, T. H. Dunning Jr and R. J. Harrison, *J. Chem. Phys.*, 1992, **96**, 6796–6806.
60 H.-J. Werner, T. B. Adler and F. R. Manby, *J. Chem. Phys.*, 2007, **126**, 164102.
61 Y. Georgievskii, J. A. Miller, M. P. Burke and S. J. Klippenstein, *J. Phys. Chem. A*, 2013, **117**, 12146–12154.
62 S. Sharma, S. Raman and W. H. Green, *J. Phys. Chem. A*, 2010, **114**, 5689–5701.
63 S. Grimme, J. Antony, S. Ehrlich and H. Krieg, *J. Chem. Phys.*, 2010, **132**, 154104.
64 T. B. Adler, G. Knizia and H.-J. Werner, *J. Chem. Phys.*, 2007, **127**, 221106.
65 G. Knizia, T. B. Adler and H.-J. Werner, *J. Chem. Phys.*, 2009, **130**, 054104.
66 F. R. Manby, H.-J. Werner, T. B. Adler and A. J. May, *J. Chem. Phys.*, 2006, **124**, 094103.
67 Y. Georgievskii and S. J. Klippenstein, *J. Phys. Chem. A*, 2003, **107**, 9776–9781.
68 H. Hippler, J. Troe and H. Wendelken, *J. Chem. Phys.*, 1983, **78**, 6709–6717.
69 C. F. Goldsmith, S. J. Klippenstein and W. H. Green, *Proc. Combust. Inst.*, 2011, **33**, 273–282.
70 M. Frisch, G. Trucks, H. Schlegel, G. Scuseria, M. Robb, J. Cheeseman, G. Scalmani, V. Barone, B. Mennucci and G. Petersson, *Gaussian 09, Revisions D.01 and E.01*, Gaussian, Inc., Wallingford, CT, 2009.
71 H.-J. Werner, P. Knowles, R. Lindh, F. R. Manby, M. Schütz, P. Celani, T. Korona, G. Rauhut, R. Amos and A. Bernhardsson, see http://www. molpro. net, 2010.
72 C. Cavallotti, M. Pelucchi, Y. Georgievskii and S. J. Klippenstein, 2018, in preparation.
73 G. B. Ellison, G. E. Davico, V. M. Bierbaum and C. H. DePuy, *Int. J. Mass Spectrom. Ion Processes*, 1996, **156**, 109–131.
74 F. Markert and P. Pagsberg, *Chem. Phys. Lett.*, 1993, **209**, 445–454.
75 R. Perry, R. Atkinson and J. N. Pitts Jr, *J. Phys. Chem.*, 1977, **81**, 296–304.
76 V. Vasudevan, D. F. Davidson and R. K. Hanson, *J. Phys. Chem. A*, 2005, **109**, 3352–3359.
77 F. P. Tully, A. R. Ravishankara, R. L. Thompson, J. M. Nicovich, R. C. Shah, N. M. Kreutter and P. H. Wine, *J. Phys. Chem.*, 1981, **85**, 2262–2269.
78 R. Knispel, R. Koch, M. Siese and C. Zetzsch, *Ber. Bunsen-Ges. Phys. Chem.*, 1990, **94**, 1375–1379.
79 O. A. Vydrov and T. Van Voorhis, *J. Chem. Theory Comput.*, 2012, **8**, 1929–1934.
80 S. J. Klippenstein, *Proc. Combust. Inst.*, 2017, **36**, 77–111.
81 D. L. Baulch, C. J. Jacobs, R. A. Cox, P. Frank, G. Hayman, Th. Just, J. A. Kerr, T. Murrels, M. J. Pilling, J. Troe, R. W. Walker and J. Warnatz, *J. Phys. Chem. Ref. Data*, 1994, **23**, 847–848.
82 M. Altarawneh, A. A. H. Al-Muhtaseb, B. Z. Dlugogorski, E. M. Kennedy and J. C. Mackie, *J. Comput. Chem.*, 2011, **32**, 1725–1733.
83 J. Zádor, S. J. Klippenstein and J. A. Miller, *J. Phys. Chem. A*, 2011, **115**, 10218–10225.

84 J. Finley, P.-Å. Malmqvist, B. O. Roos and L. Serrano-Andrés, *Chem. Phys. Lett.*, 1998, **288**, 299–306.
85 A. Hoffmann, M. Klatt and H. G. Wagner, *Z. Phys. Chem.*, 1990, **168**, 1–12.
86 C. A. Taatjes, D. L. Osborn, T. M. Selby, G. Meloni, A. J. Trevitt, E. Epifanovsky, A. I. Krylov, B. Sirjean, E. Dames and H. Wang, *J. Phys. Chem. A*, 2010, **114**, 3355–3370.
87 Y. Li, C.-W. Zhou, K. P. Somers, K. Zhang and H. J. Curran, *Proc. Combust. Inst.*, 2017, **36**, 403–411.
88 C.-W. Zhou, Y. Li, E. O'Connor, K. P. Somers, S. Thion, C. Keesee, O. Mathieu, E. L. Petersen, T. A. DeVerter and M. A. Oehlschlaeger, *Combust. Flame*, 2016, **167**, 353–379.
89 M. K. Altarawneh, B. Z. Dlugogorski, E. M. Kennedy and J. C. Mackie, *Combust. Flame*, 2013, **160**, 9–16.
90 R. A. Eng, C. Fittschen, A. Gebert, P. Hibomvschi, H. Hippler and A.-N. Unterreiner, *Proc. Combust. Inst.*, 1998, **27**, 211.
91 R. Sivaramakrishnan, personal communication.
92 P. Clothier, D. Shen and H. Pritchard, *Combust. Flame*, 1995, **101**, 383–386.
93 S. Canneaux, F. Louis, M. Ribaucour, R. Minetti, A. El Bakali and J.-F. Pauwels, *J. Phys. Chem. A*, 2008, **112**, 6045–6052.
94 C. Ellis, M. S. Scott and R. W. Walker, *Combust. Flame*, 2003, **132**, 291–304.
95 L. Elmaimouni, R. Minetti, J. Sawerysyn and P. Devolder, *Int. J. Chem. Kinet.*, 1993, **25**, 399–413.
96 F. F. Fenter, B. Nozière, F. Caralp and R. Lesclaux, *Int. J. Chem. Kinet.*, 1994, **26**, 171–189.
97 C. F. Goldsmith, L. B. Harding, Y. Georgievskii, J. A. Miller and S. J. Klippenstein, *J. Phys. Chem. A*, 2015, **119**, 7766–7779.
98 K. Hoyermann and J. Seeba, *Symposium (International) on Combustion*, Elsevier, 1994, vol. 25, No. 1.
99 H. Nelson and J. McDonald, *J. Phys. Chem.*, 1982, **86**, 1242–1244.
100 M. Pelucchi, M. Bissoli, C. Cavallotti, A. Cuoci, T. Faravelli, A. Frassoldati, E. Ranzi and A. Stagni, *Energy Fuels*, 2014, **28**, 7178–7193.
101 K. Narayanaswamy, G. Blanquart and H. Pitsch, *Combust. Flame*, 2010, **157**, 1879–1898.
102 L. Sileghem, V. A. Alekseev, J. Vancoillie, K. M. Van Geem, E. J. K. Nilsson, S. Verhelst and A. A. Konnov, *Fuel*, 2013, **112**, 355–365.